

RL-TR-96-40  
Final Technical Report  
March 1996



# ULTRAFAST OPTICAL A/D CONVERTER USING CROSS PHASE MODULATION

The City College of The City University of New York

Sponsored by  
Advanced Research Projects Agency

**DTIC QUALITY INSPECTED 2**

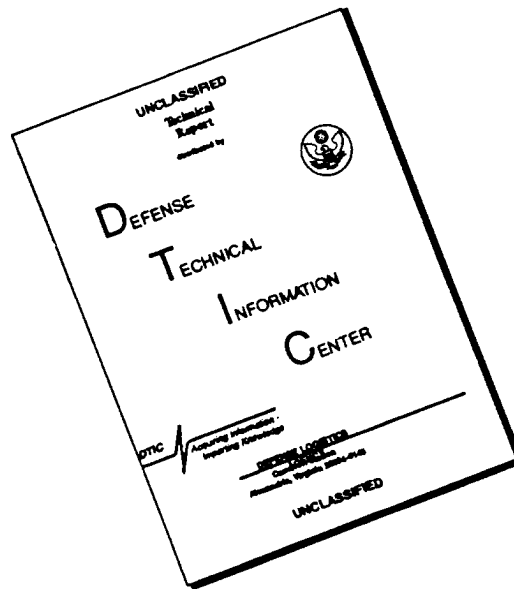
*APPROVED FOR PUBLIC RELEASE; DISTRIBUTION UNLIMITED.*

19960611 120

The views and conclusions contained in this document are those of the authors and should not be interpreted as necessarily representing the official policies, either expressed or implied, of the Advanced Research Projects Agency or the U.S. Government.

Rome Laboratory  
Air Force Materiel Command  
Rome, New York

# DISCLAIMER NOTICE

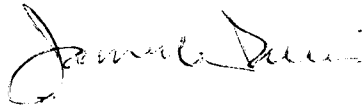


THIS DOCUMENT IS BEST QUALITY AVAILABLE. THE COPY FURNISHED TO DTIC CONTAINED A SIGNIFICANT NUMBER OF PAGES WHICH DO NOT REPRODUCE LEGIBLY.

This report has been reviewed by the Rome Laboratory Public Affairs Office (PA) and is releasable to the National Technical Information Service (NTIS). At NTIS, it will be releasable to the general public, including foreign nations.

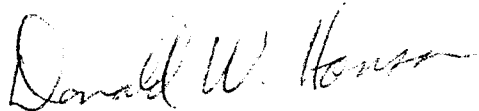
RL-TR-96-40 has been reviewed and is approved for publication.

APPROVED:



JAMES L. DAVIS  
Project Engineer

FOR THE COMMANDER:



DONALD W. HANSON  
Director of Surveillance & Photonics

If your address has changed or if you wish to be removed from the Rome Laboratory mailing list, or if the addressee is no longer employed by your organization, please notify Rome Laboratory/ ( OCPC ), Rome NY 13441. This will assist us in maintaining a current mailing list.

Do not return copies of this report unless contractual obligations or notices on a specific document require that it be returned.

ULTRAFast OPTICAL A/D CONVERTER USING  
CROSS PHASE MODULATION

P.P. Ho  
R.R. Alfano

Contractor: The City College of The City University of NY  
Contract Number: F30602-92-C-0137  
Effective Date of Contract: 17 August 1992  
Contract Expiration Date: 31 August 1995  
Short Title of Work: Ultrafast Optical A/D Converter  
Using Cross Phase Modulation  
Period of Work Covered: Aug 92 - Aug 95

Principal Investigator: P.P. Ho  
Phone: (212) 650-6960

RL Project Engineer: James L. Davis  
Phone: (315) 330-4276

Approved for public release; distribution unlimited.

This research was supported by the Advanced Research  
Projects Agency of the Department of Defense and was  
monitored by James L. Davis, RL/OCPC, 25 Electronic Pky,  
Rome NY 13441-4515.

REPORT DOCUMENTATION PAGE			Form Approved OMB No. 0704-0188	
Public reporting burden for this collection of information is estimated to average 1 hour per response, including the time for reviewing instructions, searching existing data sources, gathering and maintaining the data needed, and completing and reviewing the collection of information. Send comments regarding this burden estimate or any other aspect of this collection of information, including suggestions for reducing this burden, to Washington Headquarters Services, Directorate for Information Operations and Reports, 1215 Jefferson Davis Highway, Suite 1204, Arlington, VA 22202-4302, and to the Office of Management and Budget, Paperwork Reduction Project (0704-0188), Washington, DC 20503.				
1. AGENCY USE ONLY (Leave Blank)		2. REPORT DATE March 1996		3. REPORT TYPE AND DATES COVERED Final Aug 92 - Aug 95
4. TITLE AND SUBTITLE ULTRAFast OPTICAL A/D CONVERTER USING CROSS PHASE MODULATION			5. FUNDING NUMBERS C - F30602-92-C-0137 PE - 61101E PR - H842 TA - 00 WU - 01	
6. AUTHOR(S) P.P. Ho and R.R. Alfano				
7. PERFORMING ORGANIZATION NAME(S) AND ADDRESS(ES) The City College of The City University of New York Department of Electrical Engineering and Physics Convent Avenue & 138th Street New York NY 10031			8. PERFORMING ORGANIZATION REPORT NUMBER  N/A	
9. SPONSORING/MONITORING AGENCY NAME(S) AND ADDRESS(ES) Advanced Research Projects Agency 3701 North Fairfax Drive Arlington VA 22203-1714			10. SPONSORING/MONITORING AGENCY REPORT NUMBER  RL-TR-96-40	
Rome Laboratory/OCPC 25 Electronic Pky Rome NY 13441-4515				
11. SUPPLEMENTARY NOTES  Rome Laboratory Project Engineer: James L. Davis/OCPC/(315) 330-4276				
12a. DISTRIBUTION/AVAILABILITY STATEMENT  Approved for public release; distribution unlimited.			12b. DISTRIBUTION CODE	
13. ABSTRACT (Maximum 200 words)  This report discusses the spectral, vectorial, and temporal properties of ultrafast optical pulse propagation in single-mode optical fibers, with the objective of demonstrating and improving the spectral encoding of an optical pulse intensity using the cross-phase-modulation process for an ultrafast optical analog to digital converter. The design and test of an ultrafast analog to digital converter operating at five giga samples per second with sixteen digital levels (four bits) accuracy per sampling channel is described. Operation of the converter was demonstrated and effects limiting performance were isolated. Techniques to improve accuracy, increase sensitivity, and realize a more practical design are described.				
14. SUBJECT TERMS  Analog to digital converter, Single mode optical fiber, Modulation			15. NUMBER OF PAGES 52	
			16. PRICE CODE	
17. SECURITY CLASSIFICATION OF REPORT UNCLASSIFIED	18. SECURITY CLASSIFICATION OF THIS PAGE UNCLASSIFIED	19. SECURITY CLASSIFICATION OF ABSTRACT UNCLASSIFIED	20. LIMITATION OF ABSTRACT  UL	

## Ultrafast Optical A/D Converter Using Cross-Phase-Modulation (XPM)

### Table of Contents

	<u>page</u>
1. Executive Summary	3
2. Introduction	4
3. Review of the SPM & XPM	5
4. Design of XPM A/D	7
5. New Spectral Measurements of SPM and XPM	10
6. Spectral Encoding Algorithms	16
7. Demonstration of Unary Encoded 16 levels (4 bits) 5 GigaSamples/s A/D	24
8. Development of Compact ps/fs Semiconductor Diode Laser	29
9. Degenerate XPM and Polarization Instability	32
10. Summary: Problems and Future Direction	37
11. References	40
12. Research Staff in this Program	42
13. Accomplishments and Publication List Acknowledging RADC/ARPA	43

## 1. Executive Summary

Our research has focused on the spectral, vectorial and temporal properties of ultrafast optical pulse propagation in single-mode optical fibers with the aim to demonstrate and improve the spectral encoding of an optical pulse intensity using  $x^{(3)}$  cross-phase-modulation (XPM) process for an ultrafast optical A/D converter. In this program, the design and test of an ultrahigh speed A/D converter at Gigasamples/s with 16 digital levels (4 bits) accuracy per sampling channel using the XPM spectral encoding has been successfully demonstrated.

### APPROACH

XPM was used to encode optical pulse intensity into spectral broadening by using waveguide splitter and variable fiber lengths to obtain 50-ps time divided multiplexing (TDM) train and by using the spectral grating and streak camera to disperse (space/time) and display 5 Giga Samples/s 16 levels unary encoded signal pulses.

### KEY MILESTONES

- \* Obtained 200 channels frequency modulated XPM spectral broadening (2/93)
- \* Built a mode-locked diode laser with pulse duration  $\sim 0.6$ -ps at  $\sim 1$  GHz (12/94)
- \* Designed an ultrafast optical amplifier based on nonlinear polarization instability (6/95)
- \* Demonstrated XPM A/D of ps signal at 5 GS/s x 4 bit/s using TDM (6/95)

Under this program, seven technical papers have been published in professional journals and eight papers have been presented at professional conferences. A patent disclosure has been filed acknowledging the support of this award. This new technique, polarization controlled all-optical amplifiers, which can amplify weak optical signal to improve the sensitivity of XPM A/D and also act as ultrafast "optical transistors" for many applications has been proposed. A Ph.D. student has been trained in this program and will graduate within one year. This research has played an important role of the research and education program at CCNY. Future tasks to improve the sensitivity and accuracy of the XPM A/D include the study of the time gated XPM spectra to modify the oscillating spectra for the conversion of unary coding to priority coding, the use of circularly polarized light for the coding, the study of optical amplifier to increase the signal sensitivity, and the development of encoding algorithms to improve the bit accuracy.

## 2. Introduction

Light can be used to control light for the ultrafast optical computation and communication. Many applications have been developed, such as switches<sup>[1]</sup>, logic-gates<sup>[2-3]</sup>, amplifiers<sup>[4-5]</sup>, and multiplexer/demultiplexer<sup>[6]</sup> based on the third-order nonlinear optical processes. As the development of optical communication and information technology, the high speed optical analog to digital (A/D) converter has been drawing considerable interests. Due to its intrinsic parallel and high speed characteristics, all optical A/D converters have wide range of potential applications in optical computation. Optical A/D are needed to handle real-time data for signal processing applications such as spread spectrum communication, fiber-optic sensors. Because of the increased uses of fiber-optic sensors and fiber-optic communications, signals applied to an optical signal processor are often optical; and thus, optical A/D converter should handle optical input signals directly and be very fast.

For an all-optical A/D converter, an input light intensity analog signal is first converted into changes in certain light properties, such as the spectral distribution, through the nonlinear light-medium interaction. An encoder is then used to encode the property changes into the digital signal. Among several types of A/D converters based on different mechanism and techniques<sup>[7-11]</sup>, an all-optical A/D converter using the cross-phase modulation (XPM) for the spectral encoding is a promising one for the ultrafast applications<sup>[12]</sup>. In an XPM based A/D converter, carrier and signal light waves interact in a third-order nonlinear medium causing the phase structure of the carrier beam changed. This phase structure change imposes a change in its spectrum, or spatial distribution by a grating or a prism. This spatial distribution has the characteristics of monotonously-varying according to the light intensity with some modulation structures. A fiber/waveguide MUX/DMX unary encoder has been used to convert the spatial distribution into unary codes for A/D processing. With the advance of photonics, the improvement of the speed, sensitivity, accuracy, dimension, and cost of optical signal processing using the XPM A/D is promising.



### 3. Review of the SPM and XPM Processes

When an intense laser pulse propagating in an isotropic medium, the refractive index of the material possessing third-order nonlinearity can be written as<sup>[13]</sup>:

$$n(\omega) = n_0(\omega) + n_2(\omega) I(\omega) \quad (1)$$

where  $n_0(\omega)$  is the linear refractive index at frequency  $\omega$ ,  $n_2(\omega)$  is the nonlinear refractive index, and  $I(\omega)$  is the incident laser intensity. This refractive index change imposes a phase modulation on the laser pulses which causes spectral broadening<sup>[14-19]</sup>. When the phase modulation happens to the laser pulse itself, the process is called the self-phase-modulation (SPM)<sup>[14]</sup>. A schematic diagram of the induced phase modulation and the spectral shift from an ultrashort laser pulse with a Gaussian envelope function is shown in Fig.1 below.

Fig.1 A Schematic Diagram of  
Self-Phase-Modulation (SPM)

- (a) Self-Induced Phase Change  
(b) Induced Frequency Shift

Incident Electric Field

$$E(r,t) = E_0(t) \exp[i(\omega_0 t - k_0 z)]$$

Envelope Function

$$E_0(t) \sim A \exp(-t^2/t_0^2)$$

Incident Phase

$$\Phi(t) = \omega_0 t - k_0 z = \omega_0 t - z\omega/(c/n_0)$$

Induced Refractive index

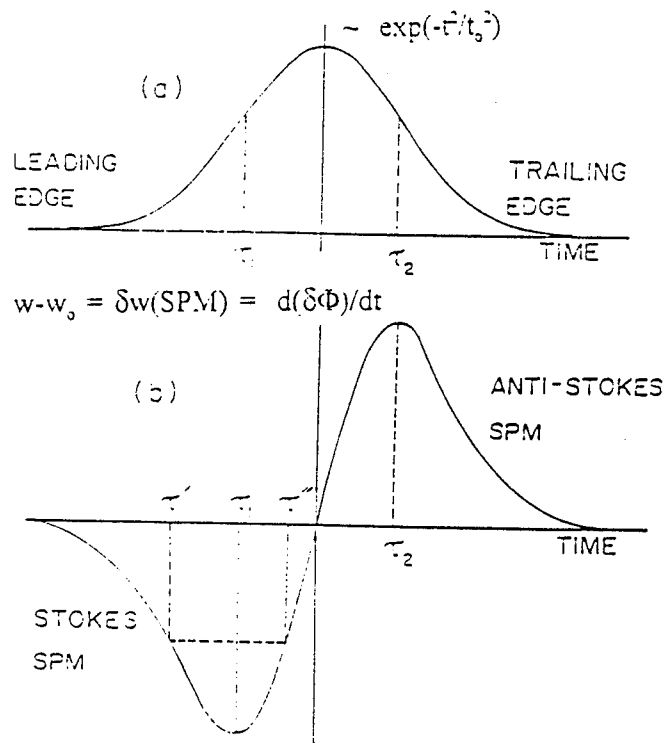
$$n(\text{SPM}) = n_0 + n_2 [E(r,t)]^2$$

Induced Phase Change

$$\delta\Phi(t) = (\omega/2c) n_2 [E(t)]^2 \sim \exp(-t^2/t_0^2)$$

Large Frequency Shift

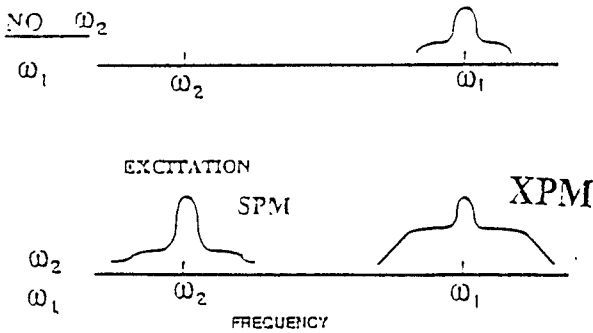
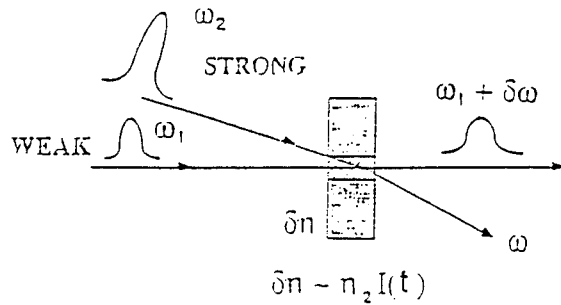
$$\omega(t) - \omega_0 = \delta\omega(\text{SPM}) = d(\delta\Phi)/dt$$



When the phase modulation occurs to two copropagating pulses, the process is called cross-phase-modulation (XPM)<sup>[20-23]</sup>. A schematic diagram of the XPM is shown in fig.2. The XPM spectral broadening of the weak probing pulse at  $\omega_2$  from an intense copropagating pulse at  $\omega_1$  :  $\delta\omega_2$  (XPM) is twice larger than  $\delta\omega_1$  (SPM).

### Cross-Phase-Modulation (XPM)

When two laser pulses propagate in matter, coupled light wave interactions occur through the third order nonlinear susceptibility  $\chi^3$ .



$$E = E_1 \exp[i(\omega_1 t - k_1 z)] + E_2 \exp[i(\omega_2 t - k_2 z)]$$

(Pump)                      (Probe)

$$n_{\omega_2} = n_0 + n_2 [E_1(r,t) + E_2(r,t)]^2$$

$$\delta\Phi_2 = \omega_2/c \int_0^L n_2 E_2^2 dz + 2\omega_2/c \int_0^L n_2 E_1^2(r,t) dz$$

(SPM)                      (XPM)

$$\delta\omega_2 = d(\delta\Phi_2)/dt$$

#### XPM Frequency Shift

$$\delta\omega(t,z) = d(\delta\Phi)/dt = 2(\omega/c) n_2 E^2 L/T_p [\exp[-(t-\tau)^2] - \exp[-(t-\tau+z/L_p)^2]]$$

Assume Gaussian Laser Input

$n_2$ : Nonlinear Index of Refraction

$E^2$ : Pump Laser Intensity

$L_p$ : Walk-Off Distance

$T_p$ : Pulse Duration

$\tau$ : Time Delay Between Pump and Probe

Fig.2 A Schematic Diagram of the Cross-Phase-Modulation (XPM) Process

#### 4. Design of XPM A/D

##### Experimental Arrangements

The experimental setup to demonstrate the XPM is shown in fig.3. A mode-locked Nd:YAG laser system with a second harmonic crystal was used to produce 39-ps 1064-nm infrared pulses and 28-ps 532-nm green pulses at 10-Hz repetition rate. The 1/e pulse duration of these two beams were measured by a streak camera system. These two beams were separated using a prism delayed scheme with wavelength selective mirrors.

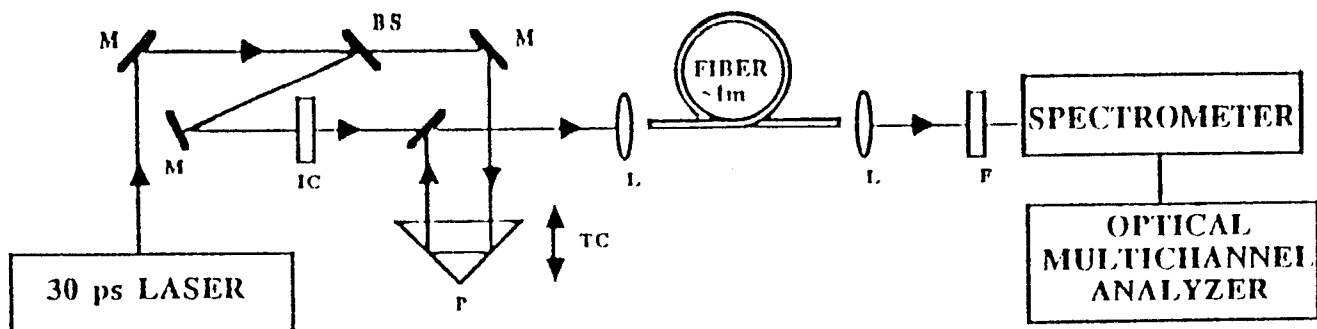


Fig.3 Schematic of Experimental XPM Arrangement

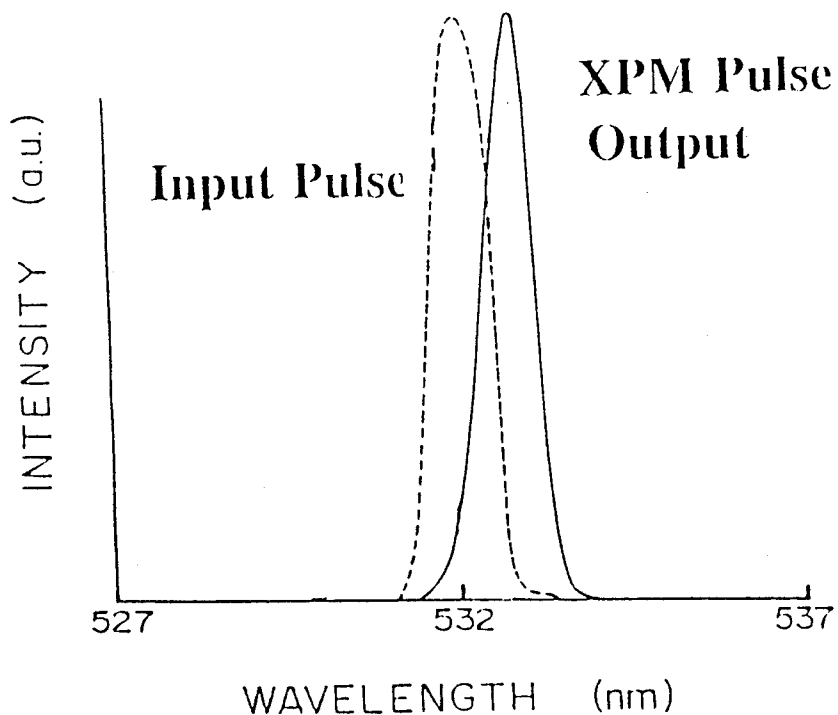


Fig.4 Preliminary Measurement of XPM Induced Frequency Shift in 1988

The 1064-nm and 532-nm pulses propagated in different interferometer arms. The optical path of each pulse was controlled by using variable optical delays. The energy of the pump 1064-nm pulses (signal to be digitized) was adjusted with neutral-density filters in the range of 1-100 nJ, and the energy of the probe 532-nm pulses (carrier) was set to be  $< 1$ -nJ. The nonlinear modulated medium was a 1-m long optical fiber with core diameter of 4- $\mu$ m, cladding diameter of 127- $\mu$ m, and numerical aperture 0.1. This 4- $\mu$ m core diameter fiber support a single mode propagation at 1064-nm and multi-modes at 532-nm laser pulses. This length was chosen to allow for total walkoff without loss of control of the pulse delay at the fiber output. The group-velocity mismatch between 532-nm and 1064-nm in fused silica was  $\sim 76$  ps/m. The output modulated 532-nm was collected by a 20X microscope objective lens. The 532-nm carrier signal after the collecting lens was split into two beams. One beam was used to into a 1-m long Jarrell-Ash spectrometer with a 600 lines/mm grating and detected by a cooled CCD camera system made by Photometrics Inc. The grating is blazed at 1- $\mu$ m. 532-nm modulated carrier signal was collect at the second order of the grating to double the spectral resolution. Using a calibration Mercury spectral lamp, the measured overall system resolution was 0.05 Å/pixel for light at 532-nm region and 0.1 Å/pixel at 1064-nm region. The manuscript entitled "High resolution spectra of SPM in optical fibers" in JOSA-B (1995) with the acknowledgement of DARPA and RADC has provided detail experimental descriptions.

Based on our preliminary measurement<sup>23</sup> in 1988 of the spectral distribution of XPM as shown in fig.4, the induced frequency shift of the probe pulse at  $\omega_2$  was found to be linearly as a function of the input pump (signal) intensity at  $\omega_1$ :  $\Delta\omega_{21}(\text{XPM}) \sim n_2 I(\omega_1)$ . Using an optical grating as a DEMUX, the output of the probing beam can be spread into a series of spatial distributed signal as a function of the input signal intensity at  $\omega_1$ . This is the basic XPM spectral encoded A/D algorithm as shown in fig.5. An equivalent optical experimental

arrangement of the XPM A/D to an conventional electronic A/D is shown in fig.6. In order to achieve 5 Gigasamples/sec and 4 bit accuracy, the time-divided XPM spectral encoded signal will be separated by an interval of 50-ps (20 GHz).

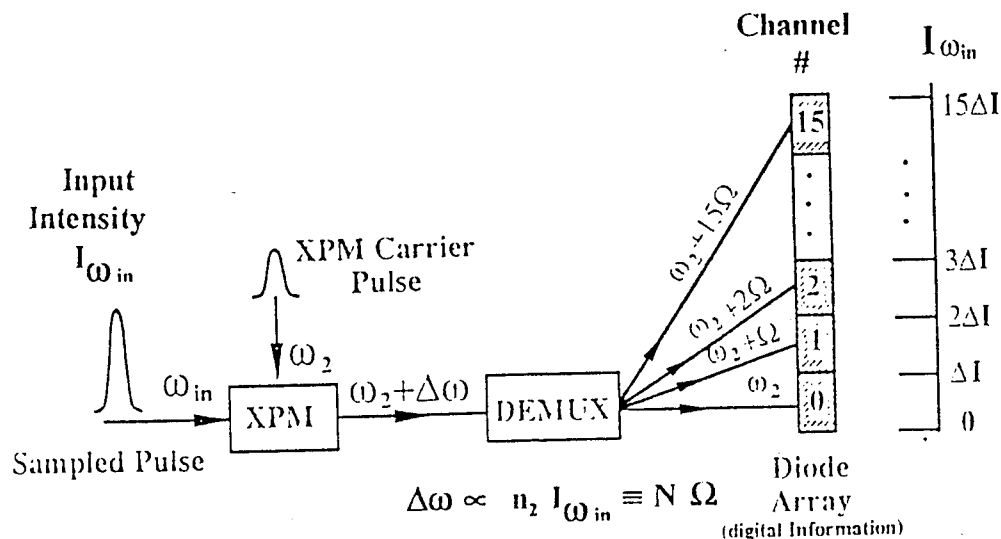
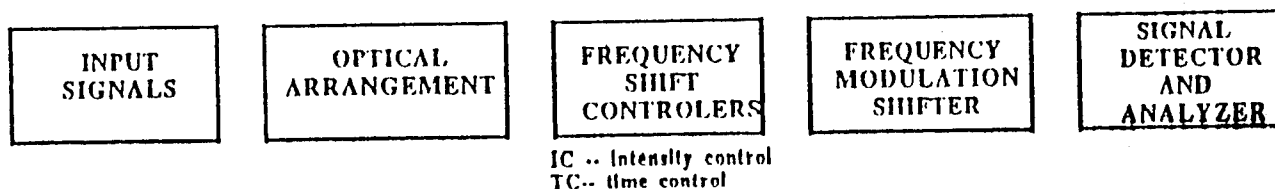


Fig.5 Schematic of a 16-digital level XPM spectral encoding algorithm



ANALOG INPUT	XPM A/D CIRCUIT	DIGITAL OUTPUT
"Intensity" of pump pulse	Optics Fibers Spectrometer	"Coded number" of frequency shifted channels

Fig.6 Comparison of optical A/D algorithm to conventional electronic A/D algorithm

## 5. New Spectral Measurements of SPM and XPM

### i) Picosecond Measurements

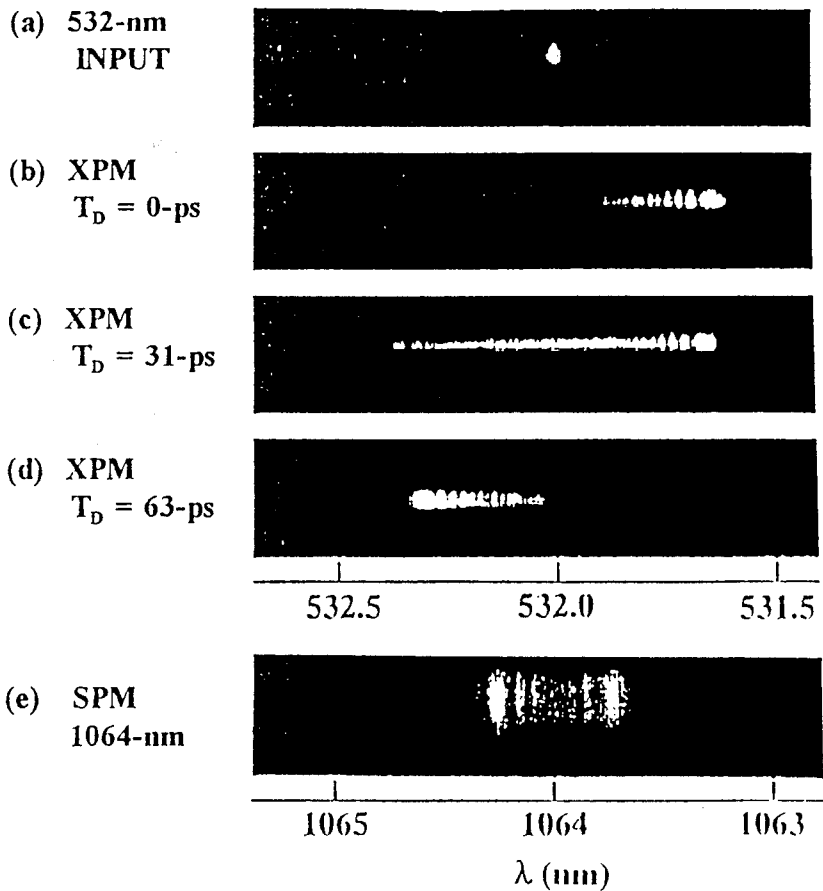
We have repeated the SPM and XPM experiments and have improved the XPM shifts from 10 channels obtained in 1989 up to 300 channels. Typical measured 2-D spectra of SPM and XPM are displayed in fig.7. This improvement of shifted channel numbers between fig.7 to our previous measurement in fig.4 was achieved through the combination of the following three factors: small pixel size of CCD camera, doubled the line numbers per mm of the spectral grating, and the use of second order of the grating.

Fig.7. Measured SPM and Time-resolved XPM Spectra through a 5- $\mu$ m diameter fiber. Pump pulse:1064-nm. Carrier pulse: 532-nm.  $T_D$ : time delay between 1064-nm to 532-nm pulses.

- (a) Input 532-nm spectrum
- (b) XPM(532-nm):  $T_D=0$ -ps
- (c) XPM(532-nm):  $T_D=31$ -ps
- (d) XPM(532-nm):  $T_D=63$ -ps
- (e) SPM of 1064-nm

The spectral width of input 532-nm carrier pulse was  $\sim 0.2$ -A. The improvement of the spectral resolution is attributed from the following arrangements.

	<u>Past</u>	<u>Now</u>
Detector	OMA	CCD
Signal	1-D/2-D	2-D
Wavelength	0.4-0.8 $\mu$	0.4-1.1 $\mu$
Resolution	0.5 A	0.05A



Computer simulations were used to numerically produce the modulated XPM spectrum as a function of the signal intensity level. Using a mode-scrambler to reduced spatial mode propagation of 532-nm pulse in fibers, clean XPM spectra was obtained as displayed in fig.7. The 1-D digitized intensity profile of the measured time-resolved XPM spectra is displayed in Fig.8. The theoretical curves from the computer numerical calculation of these XPM spectra displaced in the right column of fig.8 have an excellent fit to the measured XPM curves in the left column of fig.8. From both figs.7 and 8, fine modulated oscillatory XPM spectra can be observed due to the improved spectral resolution down of 0.05A. When the 532-nm carrier pulse energy was kept constant, as 1064-nm pump pulse (signal to be digitized) energy was increased, the spectrum of the output carrier pulse was shifted further to the Stokes side and the oscillation periods increased. The previously designed binary A/D encoding algorithm needs to be modified due to the new oscillation feature (see chapter 6)

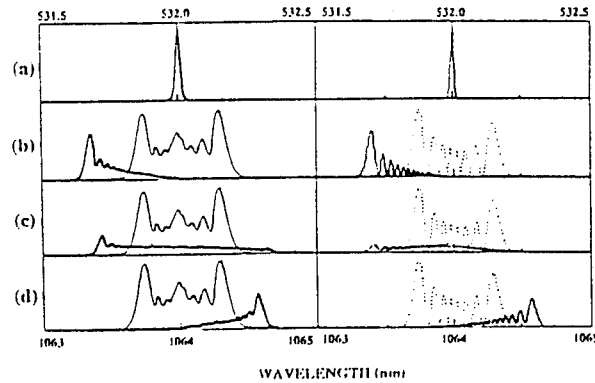


Fig. 8. SPM of the pump pulse at 1064 nm and XPM spectra of the probe pulse at 532 nm propagating in an optical fiber with different initial time delays. The left-hand column shows the experimental results, and the right-hand column shows the theoretical calculations. The core diameter of the optical fiber was 4  $\mu\text{m}$ , and  $n_2 = 3.2 \times 10^{-16} \text{ cm}^2/\text{W}$  for 532 nm and  $n_2 = 1.79 \times 10^{-16} \text{ cm}^2/\text{W}$  for 1064 nm. (a) Input laser pulse, (b)  $t_d = 0$  ps, (c)  $t_d = 31$  ps, (d)  $t_d = 63$  ps. The peak power of the pump pulse is 2000 W.

Measurements of 16 level (4bits) resolution have been obtained. Sixteen modulated spectrographs of 532-nm beam modulated by sixteen different pump 1064-nm intensity levels are shown in fig.9. A plot of induced wavelength shift as a function of the input 1064-nm laser intensity is shown in fig.10.

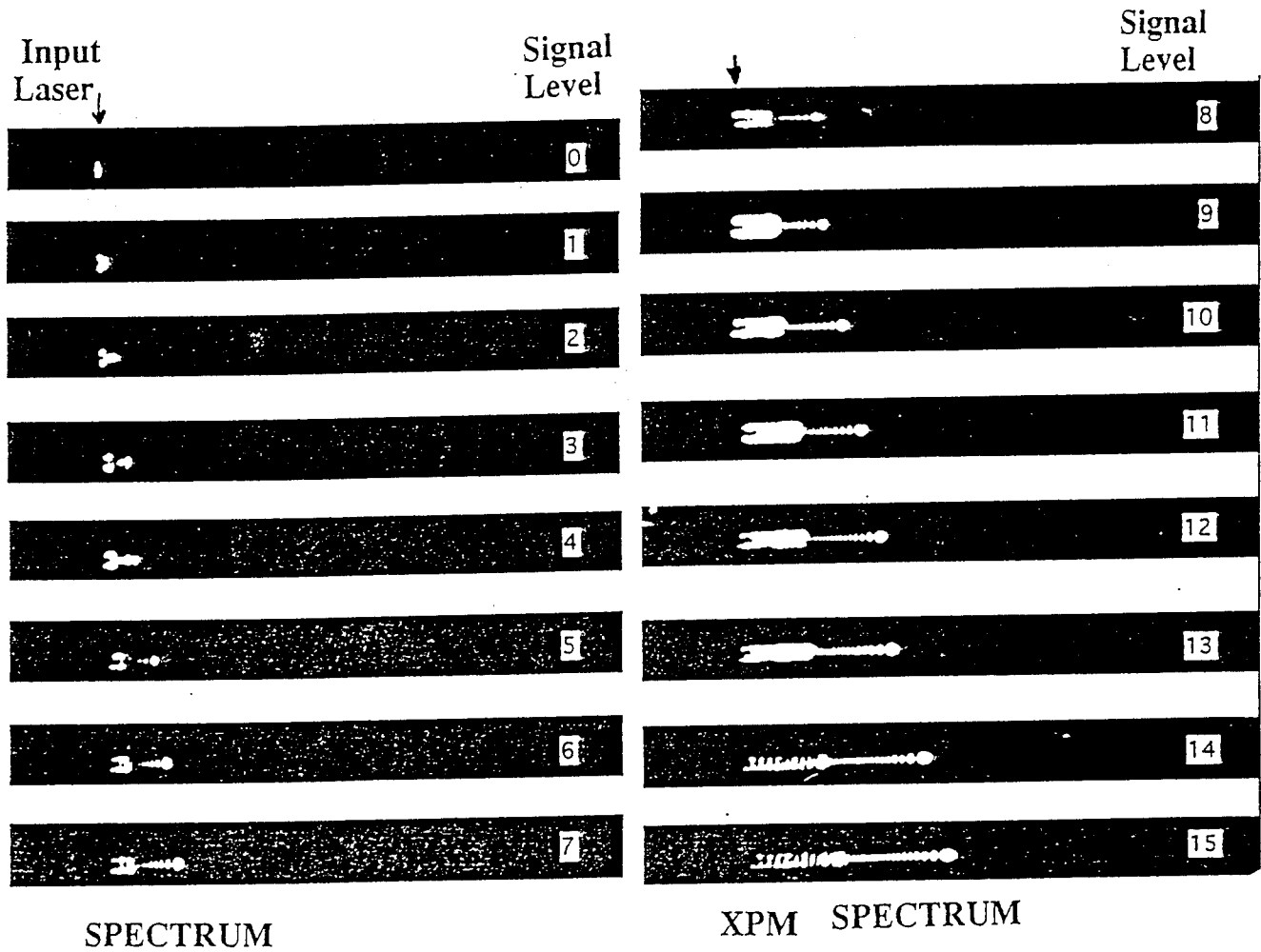


Fig.9 Measured XPM spectra of 532-nm with equivalent 1064-nm signal level from 0 -> 15.

The input carrier laser pulse at 532-nm was modulated by a simulated signal from 1064-nm laser pulse. The measured output spectra of the 532-nm pulse from the CCD camera was broadened to ~ 170 channels.



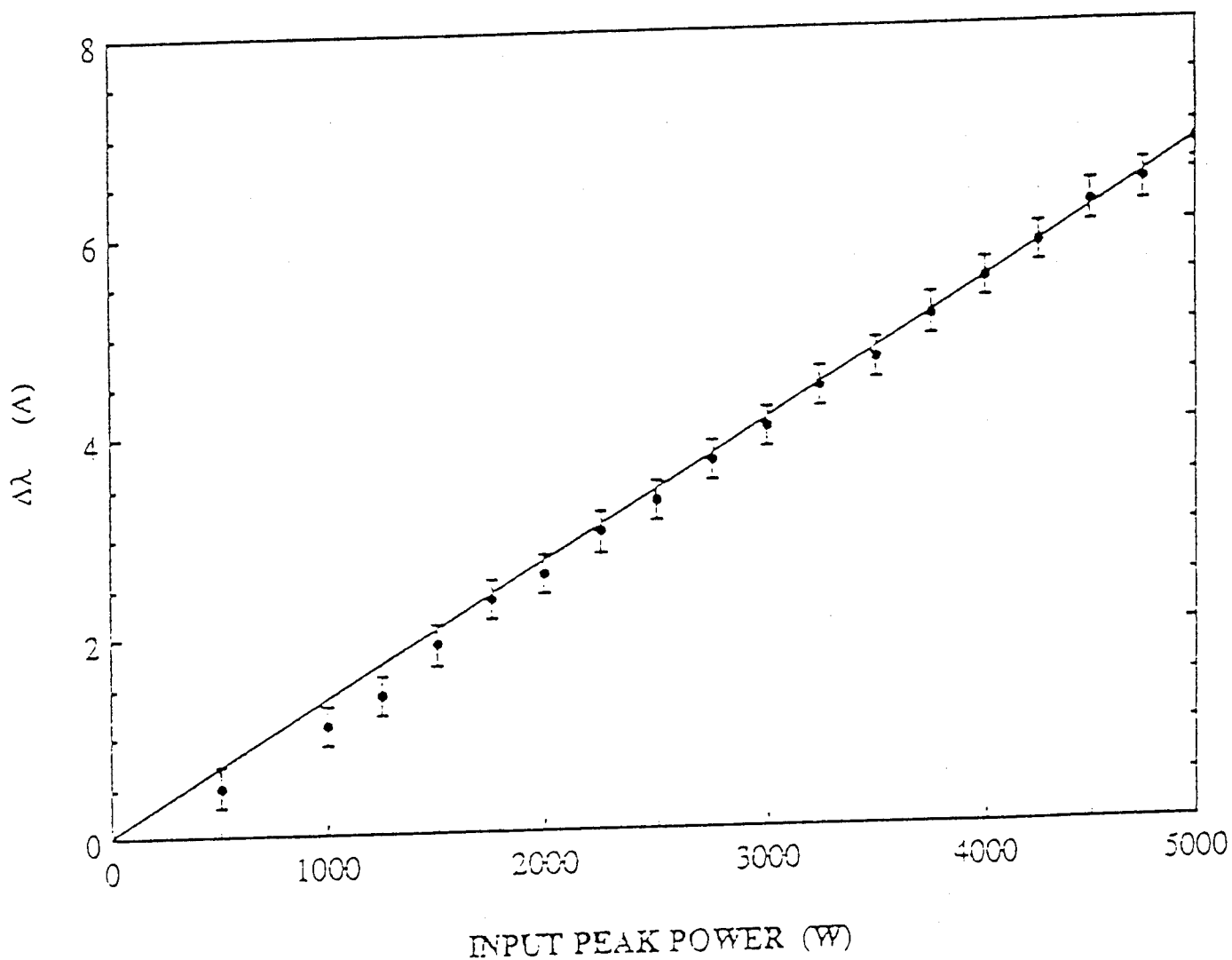


Fig.10 Linearity of XPM spectrum as a function of the input 1064-nm peak power.

The spectral resolution of the CCD spectrograph was 0.05-Å. The spectral width of input 532-nm carrier pulse was 0.2-Å. Each data point was an average of 4 to 6 shots. The fluctuation of input signal energy of 1064-nm pulse was  $\sim \pm 6\%$ . The measured fluctuation of the spectral shift of 532-nm was  $\sim \pm 0.3$ -Å.

## ii) Femtoseconds SPM and XPM Measurements

Using a femtosecond Ti:sapphire laser system, the SPM and XPM spectra have also been measured as shown in fig.11. The output of the Coherent MIRA Ti-sapphire laser was center at  $\sim 780$ -nm with 6-nm bandwidth, 80-fs duration, 76-MHz pulse repetition rate, and 20-nJ pulse energy. Through a fiber with length varied from 10-cm to 1-m, both the SPM and XPM spectra have been obtained. XPM spectrum was obtained using the degenerate-XPM (DXPM) where two pulses (one intense pulse as the pump and one weak pulse as the probe) both at 780-nm but with perpendicular polarizations were used. The broadened spectra were found to be slightly deviated from the input signal intensity which may be attributed to the induced polarization change.

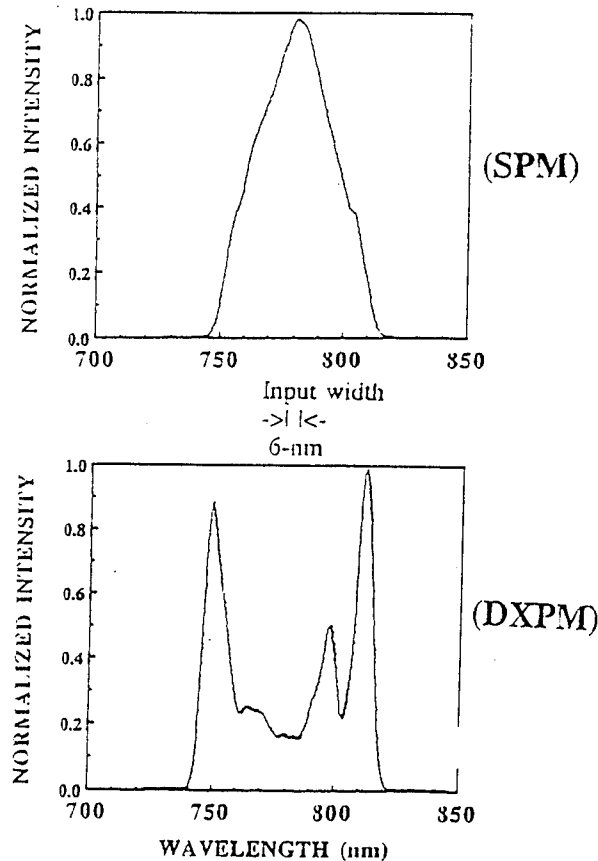


Fig.11 Femtosecond SPM and DXPM spectra of  $\sim 10$ -nJ 80-fs laser pulses at 780-nm wavelength propagating through an 1-m long isotropic single mode fiber.

In addition, the linearity of the spectral broadening bandwidth  $\delta\omega$  was measured as a function of the incident Intensity for both SPM and DXPM from a range of fs pulse energy from 0 - 8-nJ as shown in fig.12. The output band width was increased to  $\sim 80$ -nm (ps laser experiment, the bandwidth was  $\sim 1$ -nm). Due to the input bandwidth of  $\sim 6$ -nm, the maximum possible digitized level remains to be less than 16 (4 bits). In addition, the linearity of the  $\delta\omega$  was found to be much worse than the results from the ps measurement. The nonlinearity saturation behavior can be accounted for the dispersion and energy spread through a larger bandwidth at higher energy input. The effective spectral intensity was reduced. To minimize the dispersion effect, the effective fiber length used for fs DXPM has been measured. The spectral broadening saturation occurred when the fiber length was longer than 10-cm at 8-nJ input energy.

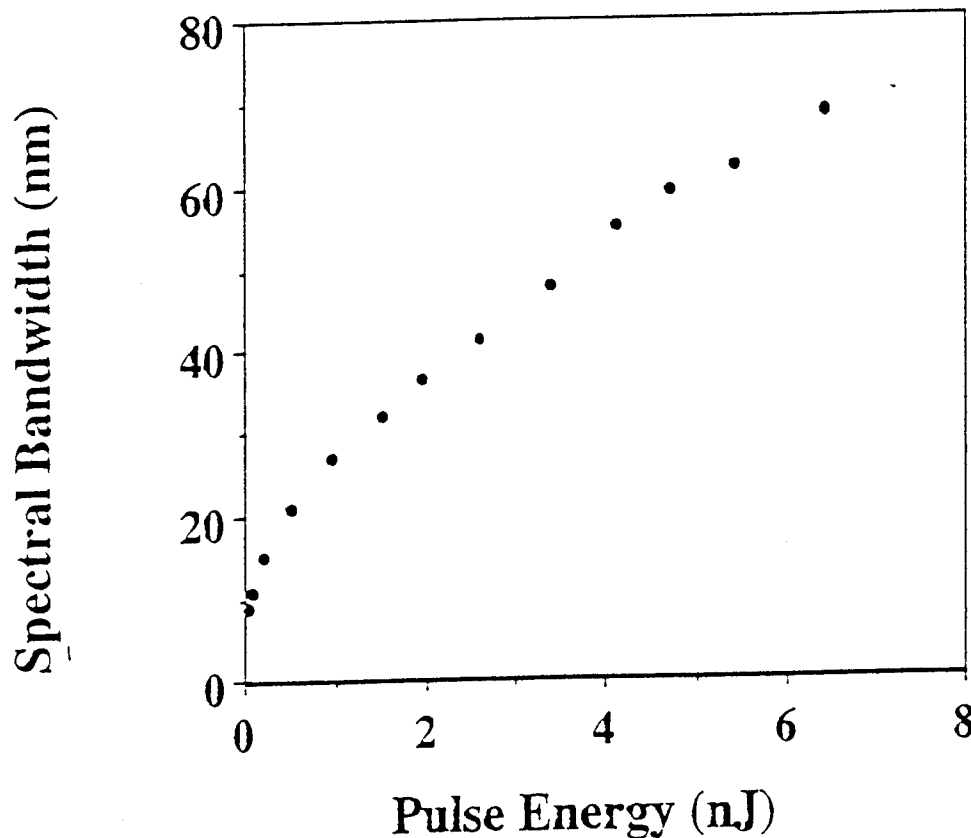


Fig.12 Measured Intensity Induced Spectral Broadening of fs Laser Pulses in Fibers

## 6. Spectral Encoding Algorithms

From our preliminary measurements in 1988 of the induced frequency shift of XPM in fig.4, a binary encoding algorithm schemes was proposed as shown in fig.13a to convert the 16 digitized spectral levels into a 4-bit signal using a mechanical mask. In addition, using a fiber and waveguide MUX/DMX, similar binary conversion can also be achieved as shown in fig.13b.

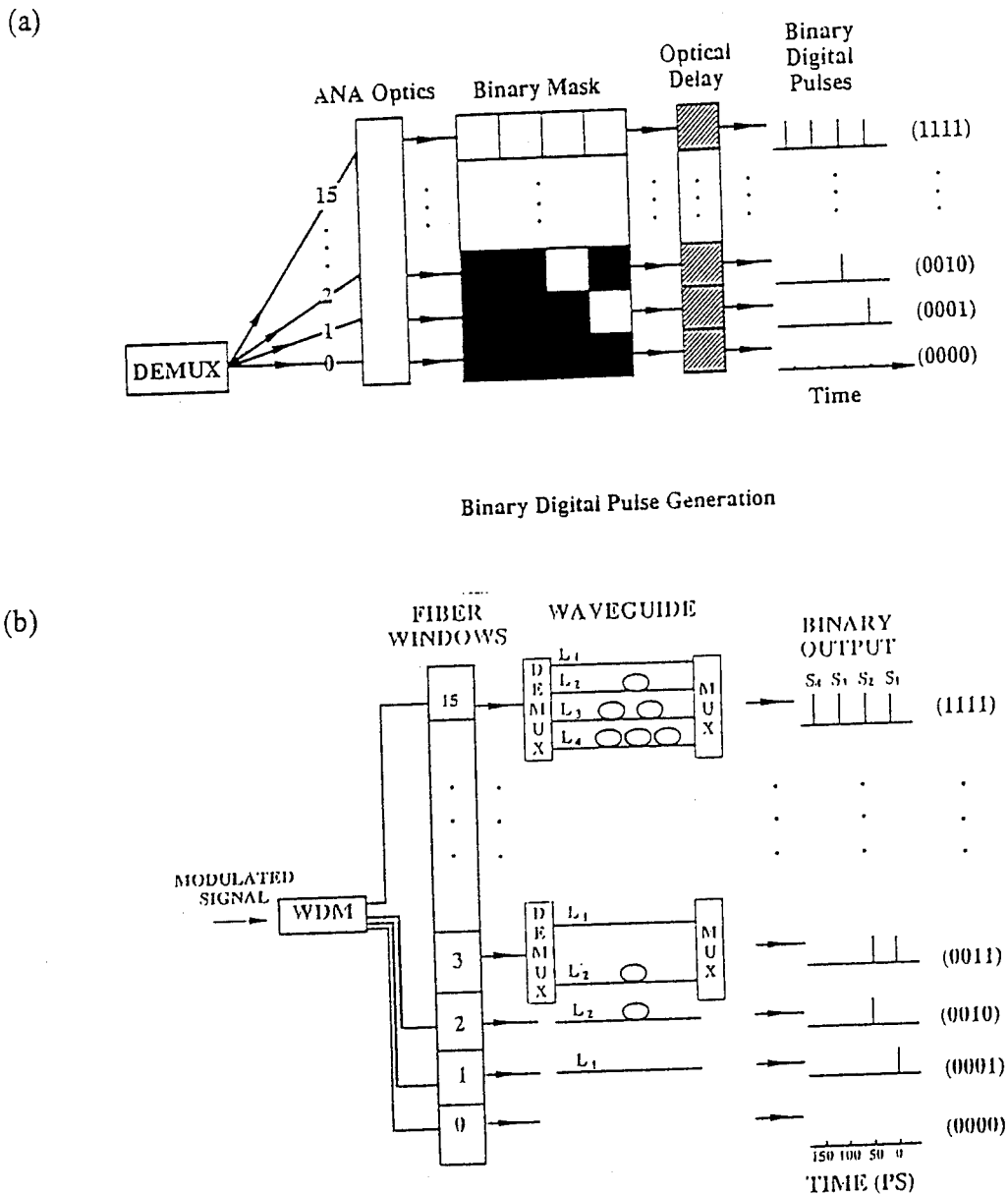


Fig.13 Schematic Design of Binary Encoding Algorithm to Convert 16-digitized levels to 4-bit

However, from our new measurements and theoretical simulations shown in figs.7 and 8, the cross-phase-modulation spectra displayed an oscillatory feature. This oscillatory phenomenon may be adaptable for the high bits A/D converter. Various encoding algorithms have been investigated. Encoding uses various high/low frequency variation at different induced frequency locations for A/D. For example, a modulated spectrum shown in fig.7 can be represented as a 13 bit digitized signal as 010,101,010,111,0. Each maximum above a given threshold intensity level is coded to be 1. This is different to our previous approach using the averaged value of  $\sim 7$  channels shift which represents  $\sim 3$  bits. This encoding algorithm could be enveloped in a future project. The followings will discuss the study of using the Fourier spectral filtering to modify the oscillatory spectra into a single sharp signal for the priority coding and the unary encoding technique used for the final demonstration.

#### i) Fourier Spectral Filtering to Modify Oscillatory Spectra into a Singular Data

In order to digitize this complex modulated XPM spectrum for our previous planned binary encoding, an optical filter/mask is needed to convert the output spectrum into a single well defined source. A preliminary calculation using Fourier optical filtering, a simulated modulated input can be Fourier transformed into a well defined spectral signal as shown in fig.14 below. Fig.14a represents a simulated 2D oscillatory XPM spectrum, after passing through a designed spatial mask located at the Fourier plane as shown in fig.14b, the output signal in fig.14c has shown a singular peak as we desired for the original A/D design shown in fig.4. The Fourier spatial filter was designed by solving the inverse Fourier transformation from the desired singular output of fig.14c to the known oscillator input of fig.14a.

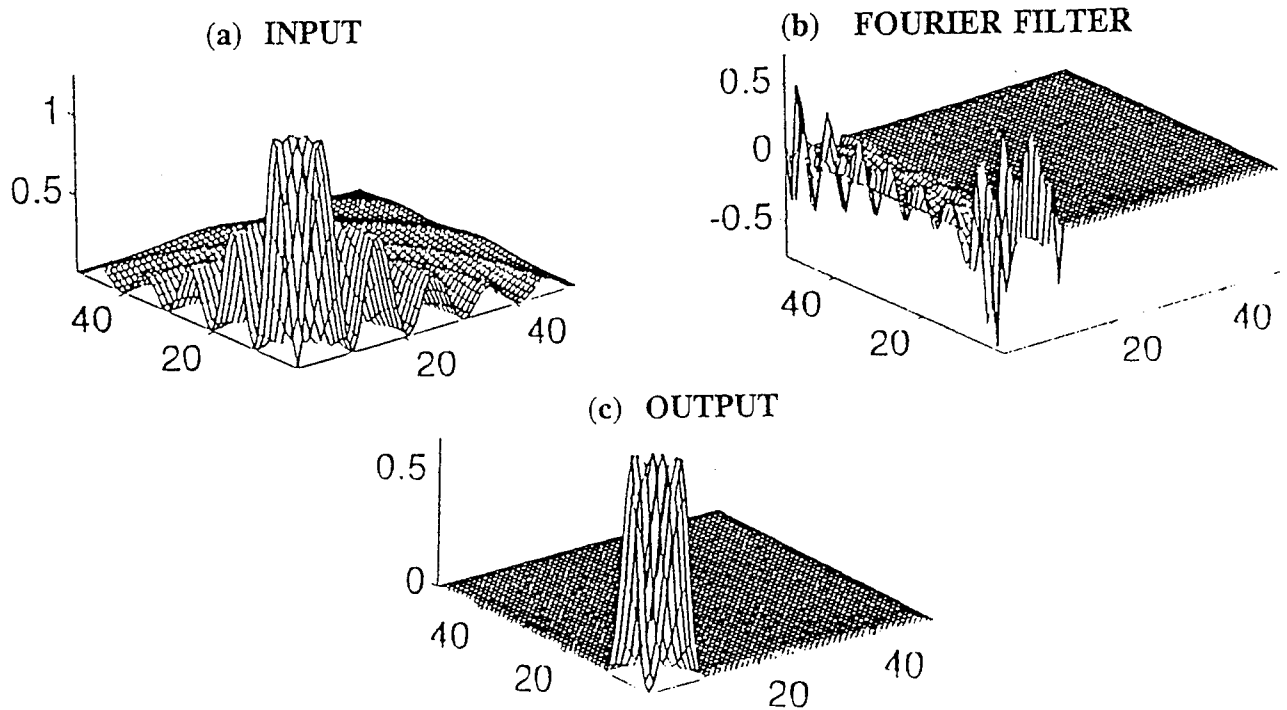


Fig.14 Computer Simulation to Transform a 2D Modulated Spectrum Into a Discrete Signal

- (a) Input Modulated Signal with Modulated Intensity 2D Spatial Distribution  
 (b) Fourier Spatial Filter Arrangement (c) Output Singular Signal to be Digitized

Optical Priority Encoding To digitize the transformed signal from the XPM spectrum shown in fig.14c, beside our previous binary encoding scheme, there are several other approaches to encode the broadened XPM spectrum, such as priority encoding, unary encoding, and Chinese remainder encoding. The optical priority encoding to digitize the modulated XPM spectrum has been studied. Priority encoding is a popular technique in conventional electronics. This encoding ensures that only the highest order data line to be encoded. The encoding function table for a typical electronic application of a three bit system with values of 0, 1, 5 is shown in fig.15.

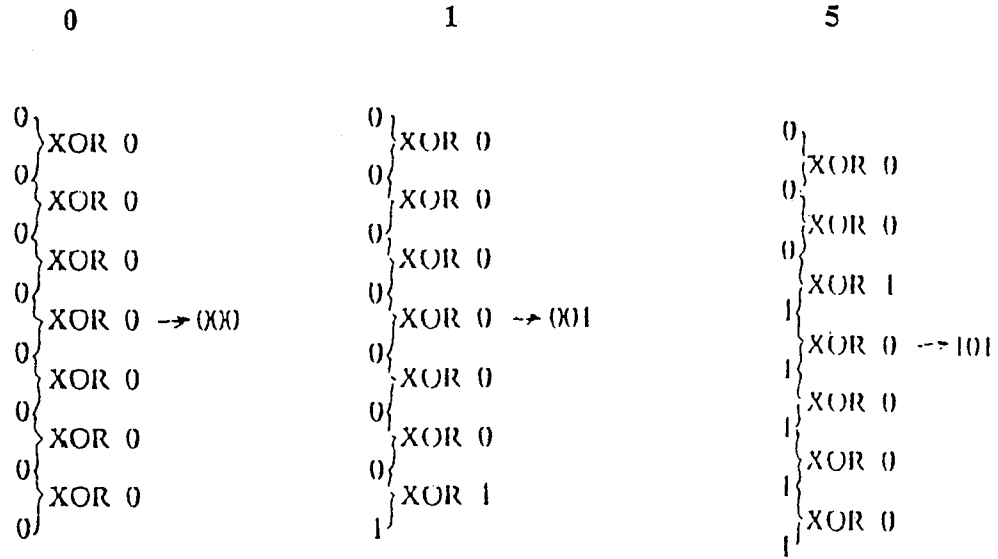


Fig.15 3-bit Priority Encoding Function Table

In fig.15, the input electronic signals are encoded using XOR gates. For optical signals, an equivalent XOR function can be replaced with a Fourier optical differential operation. A schematic diagram of the Fourier differential of an amplitude signal  $g(x,y)$  is illustrated in fig.16 using a 4F optical system. Right in front of the back focal plane (mask location), the illumination light through  $g(x,y)$  after the lens  $L_1$  is Fourier transformed to

$$G(x,y) = F\{g(x,y)\} \quad (2)$$

For the derivative along the x-direction, a phase mask of  $j2\pi f_x$  will be used, where  $f_x = x/\lambda f_1$ .

After the mask, the transmitted signal can be written as

$$G'(x,y) = j2\pi f_x G(x,y) \quad (3)$$

After the second lens  $L_2$ , the masked  $G'(x,y)$  will be Fourier transformed to the derivative

$$\text{form of } g'(x,y) = d g(x,y)/dx = F\{G'(x,y)\} \quad (4)$$

at the location of the second back focal plane at the screen. The image obtained on the screen is invertly magnified by a factor of  $f_2/f_1$ , where the inversion occurs from the operation of FF instead of  $F^{-1}F$ .

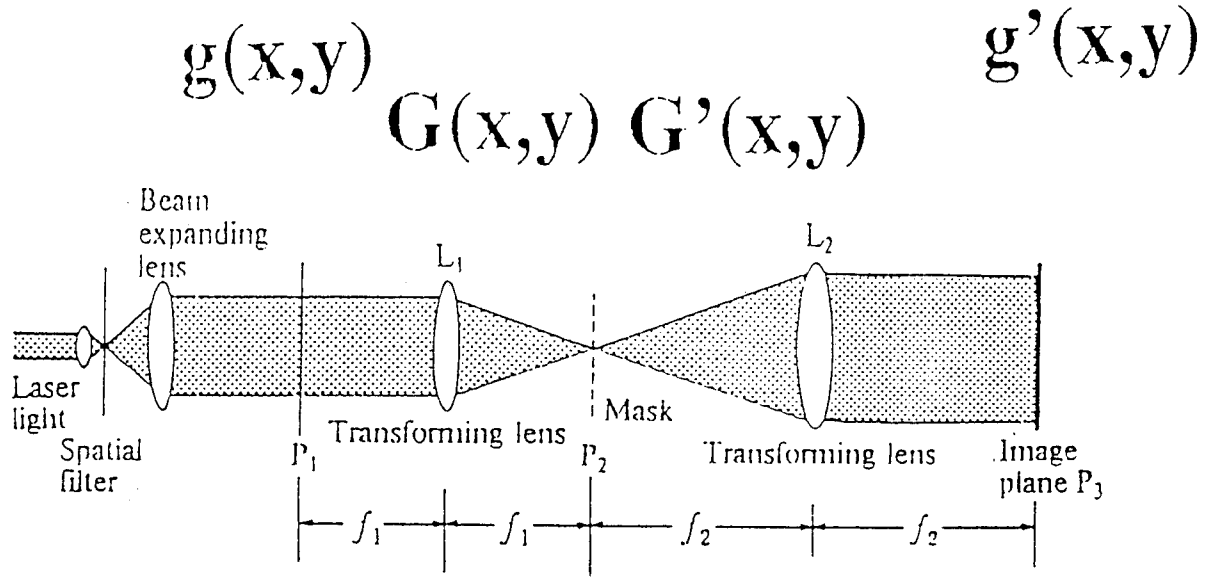


Fig.16 Experimental Arrangement of Optical Fourier Differentiation

To apply this Fourier differentiation operation, a simulated 1D optical signal shown in fig.14a,  $g(x)$ , of a broadened XPM spectrum coming out from the spectrometer where the horizontal axis  $x$  is the wavelength will be sent through the 4F system in fig.16. After the Fourier differentiation, the 1D digitized output signal,  $g'(x)$ , at the image screen can be represented as shown in fig.17b. Most output energy is concentrated at the high wavelength end. This optical Fourier differentiation operation is similar to the electronic priority encoding.

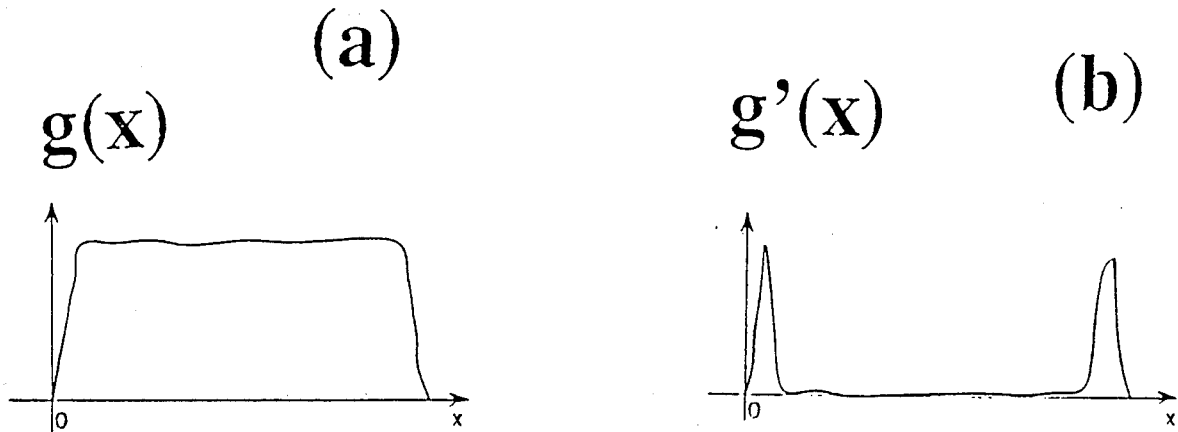


Fig.17 Simulation of Fourier Differentiation of 1-D Broadened Optical Spectrum  
 (a) Input signal  $g(x)$  (b) Output signal  $g'(x)$



After the differentiation, the standard binary encoding approach can be applied. An example of a 3-bit optical priority encoding is shown in fig.18. In this proposal, the student will learn and design various phase masks to convert broadened and modulated XPM spectrum to a binary form with minimum power loss.

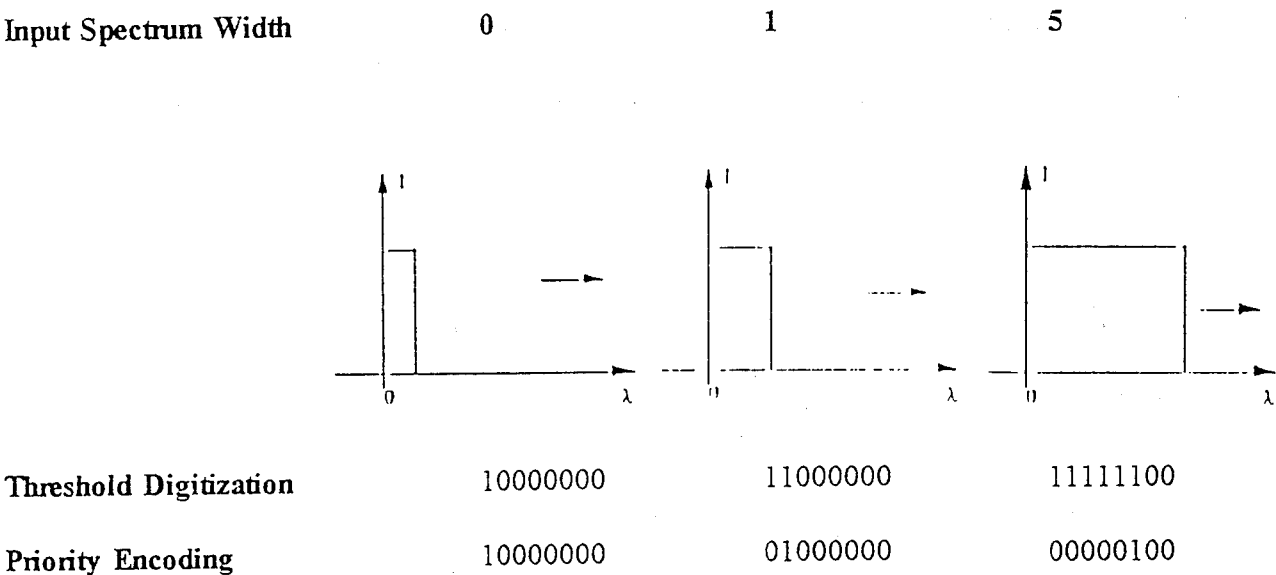


Fig.18 Example of 3-bits Optical Priority Encoding for three spectrum: 0, 1, and 5

To obtain the optical differential for the priority encode of XPM spectrum, phase masks are needed at the Fourier plane. Various phase masks will be designed and tested. For example, a  $j2\pi f$  mask has the values from negative to positive. This kind operation can be obtained from the following two operations of the amplitude transmission function  $|2\pi f|$  and the sign filter. The sign filter function can be accomplished by a phase retardation plate. This phase plate is a dielectric coated optical flat with one-half of the plate has a phase retardation of  $n\pi$  rad ( $n$  is an odd integer). The amplitude transmission function can be approximated obtained using a transparent slide made from a fine grain 35-mm photographic film. The Fourier transformed XPM signal can convert the energy from the spread spectrum into a well defined wavelength with minimum loss of energy for the designed digitization algorithm.

## Unary Encoding

The above Fourier filtered spectral modification approach works in theory. However, it is difficult to implement in terms of the filter fabrication. At present, a simplified unary encoding scheme has been adapted for the demonstration of XPM digitization project. For the unary code, each bit represents either 0 or 1 and the final number is a simple summation of the non-zero bit. A time-divided multiplexing unary encoding algorithm for a ps XPM A/D is shown in fig.19.

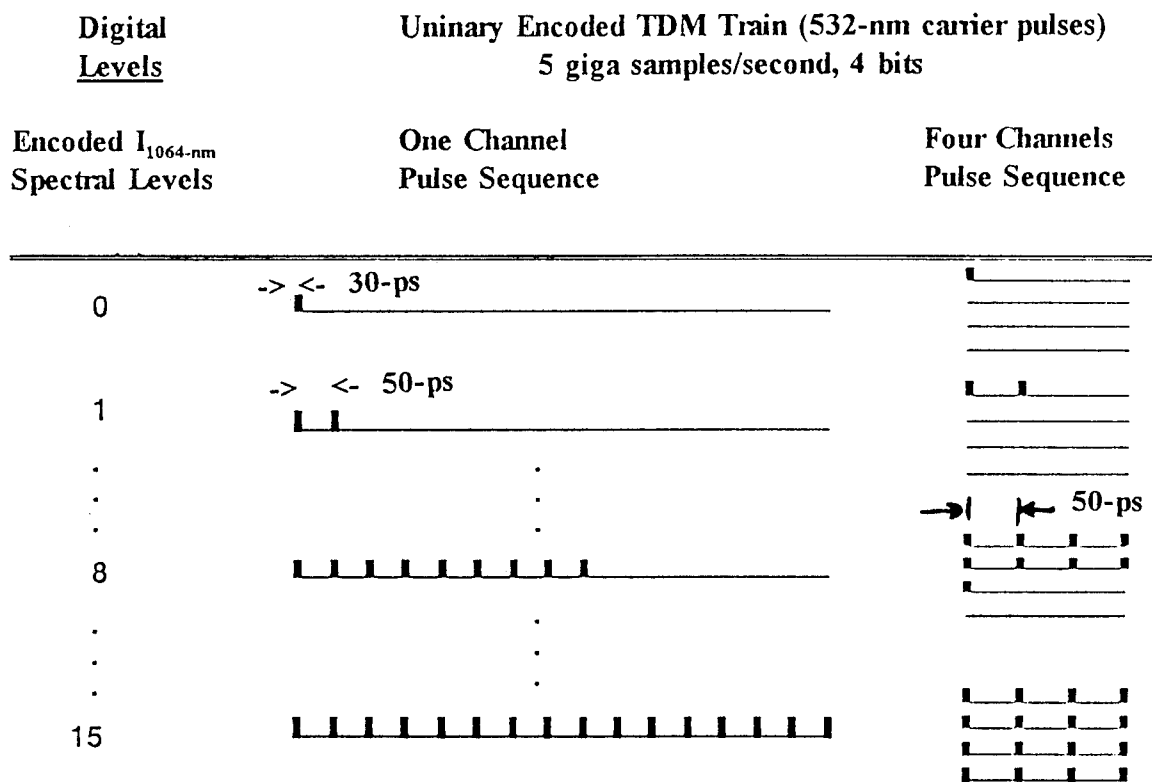


Fig.19 16-level Time-Divided Multiplex (TDM) Unary Encoding  
1 Channel (16x1) and 4 Channels (4x4) fiber/pulse sequence approaches.

The input signal at 1064-nm will be digitized into a 16-level unary code from 0 to 15. Since the laser pulse duration is 30-ps, the fast repetition rate between two adjacent pulses is limited to ~ 50-ps. For a one-channel approach, the total time to encode a 16-level signal will be

$16 \times 50\text{-ps} = 800\text{-ps}$ . This 800-ps will greatly slow the sampling rate. To increase the sampling rate, multi-channel parallel data transmission lines can be used. For instance, using a 4-channel approach, the total sampling time can be reduced by a factor 4 to 200-ps or 5 Gigasamples/sec. As long as the space allowed, theoretically, a 1000-channel (10 binary bits) TDM unary encoding can be implemented. For this A/D demonstration, the XPM temporal-spectral unary encoder has been assembled with a set of 16 optical fibers as shown in fig.20. 16 fibers were coupled to the output of a spectrometer (MUX). Every four fibers are formed a set to be combined using a 4x1 waveguide DMX into one data line. The length between these four fibers in each of the fiber set has been cut to be  $Z$ ,  $Z+\Delta$ ,  $Z+2\Delta$ ,  $Z+3\Delta$ , respectively. Where the fiber length difference  $\Delta$  was set to be 1-cm which corresponded to a 50-ps optical time delay. This encoder will be used in the 16 level 5 Gigasamples/sec XPM A/D demonstration.

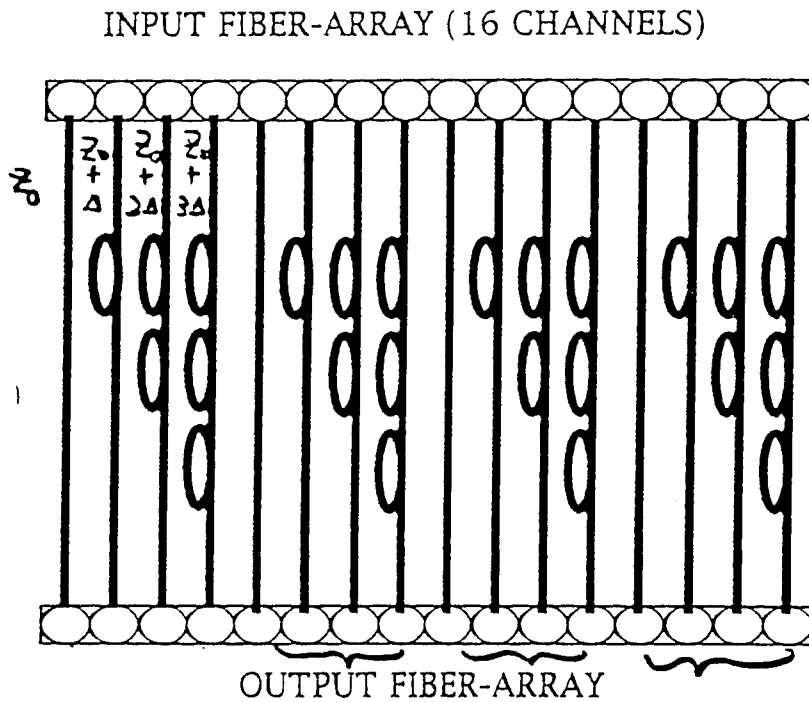


Fig.20 16 Level (4 bits) Temporal-Spectral Unary Encoder

## 7. Demonstration of 16 levels (4 bits) 5 Giga samples/sec XPM A/D

A schematic of the experimental setup to demonstrate the 4-bit digitization of a sampled ultrafast optical pulse using a 50-ps time divided multiplexing train and the spectral grating/streak camera to display 5 Gigasamples/sec 16-levels unary encoded XPM optical signal pulses is shown in Fig.21. A 30-ps at 532-nm laser pulse was used as the carrier source and 30-ps 1064-nm laser pulse was used as the signal pulse to be digitized.

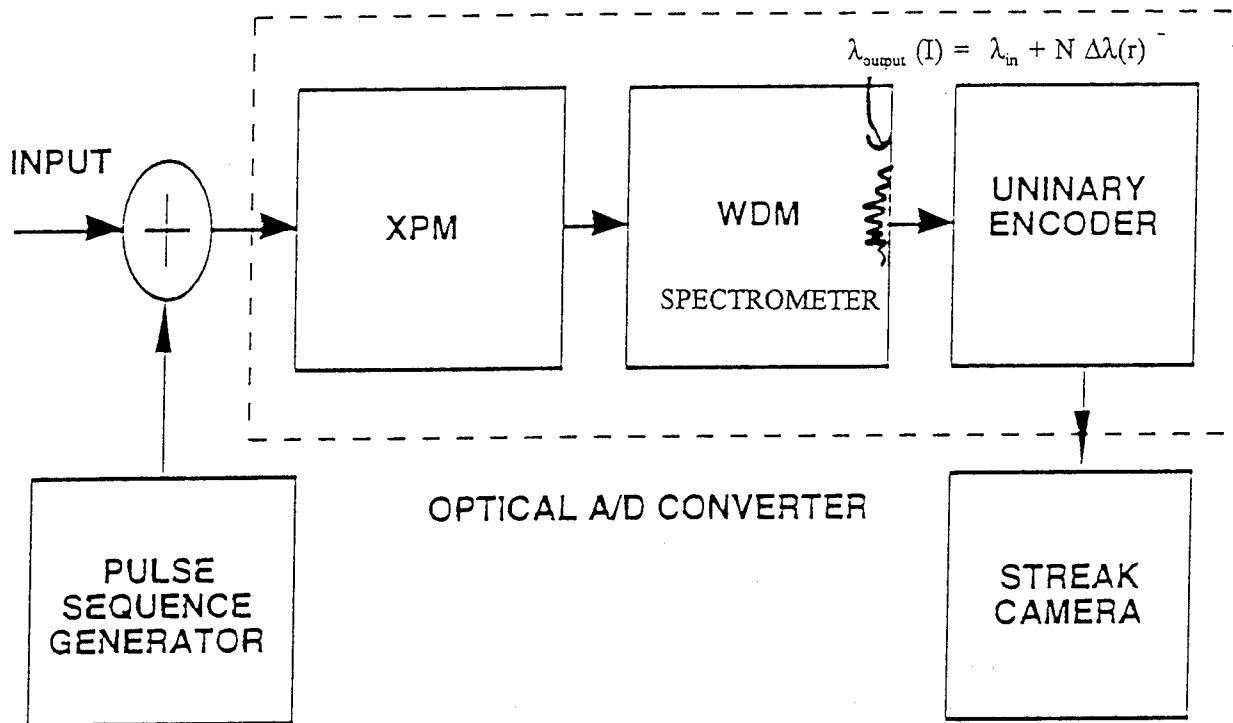


Fig.21 Schematic Diagram of an 5 Gigasamples/sec 16-level XPM A/D

Input: 30-ps pulses at 532-nm/1064-nm (carrier/signal) from a mode-locked Nd:YAG laser

Pulse Sequence Generator: split a 30-ps into a four 30-ps pulse train separated by 50-ps  
(see fig.22 and 23 for separate diagrams)

XPM: 1-m long single-mode fibers for XPM process of 532/1064-nm pulses

WDM: 1-m Jarrell-Ash spectrometer to disperse spectral broadened 532-nm XPM pulse

Unary Encoder: variable length fiber bundles and waveguide MUX/DMX (figs.19,20)

Streak Camera: 2D image with 10-ps resolution to demonstrate XPM encoded TDM

To simulate a signal to be sampled, a single shot pulse was broken into a 3-pulse train using either a conventional beam splitter optics as shown in fig.22. With the proper design of the mirror reflectivity as shown in fig.22, the pulse intensity from each pulse of the carrier train was equal while the intensity of the signal train was set to be 6:2:1.

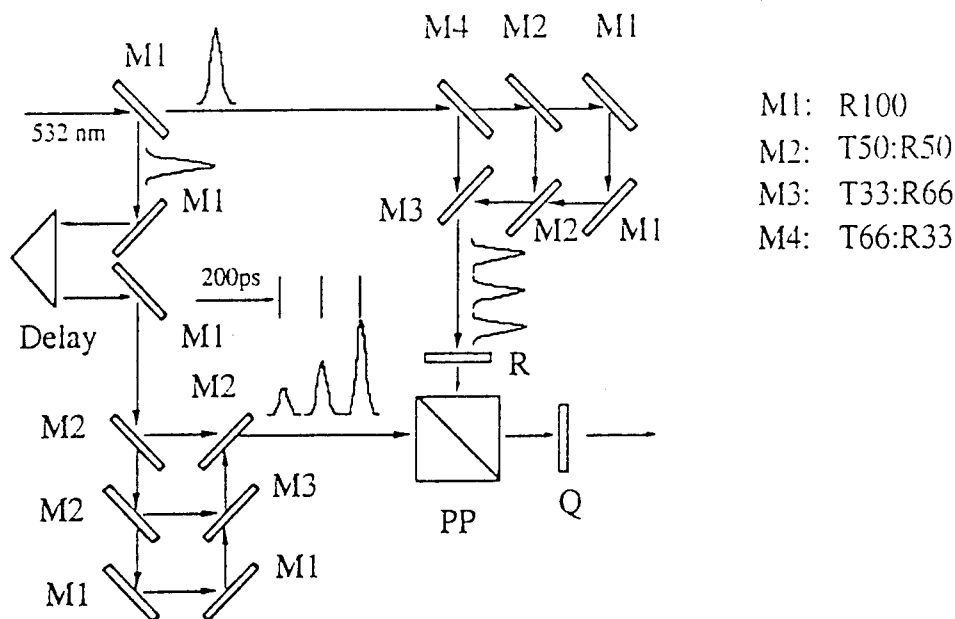


Fig.22 A Schematic Design of Optical Sampling and Clock. An input pulse into two 3-pulse trains with intensity distribution for the carrier train as 1:1:1 and for the signal train as 6:2:1

The design in fig.22 was bulky and expensive. This concept was not used. In this XPM A/D demonstration, a new design using the variable fiber lengths and waveguide DMX (splitter) and MUX (coupler) as shown in fig.23 was used to create a 4-pulse train to simulate the sampling process with much less cost and space. At the moment, one problem to use the fiber/waveguide pulse sequence generator is the control of the intensity splitting. Since the manufacture specifications of most commercial available fiber/waveguide splitter/couplers are designed for 1330-nm and 1550-nm wavelengths, the intensity distribution at 532-nm and 1064-nm, especially, 532-nm were quite different to the value from the catalog purchasing. The intensity distribution ratio of the splitter/coupling was experimentally measured. A photograph of the experimental arrangement of the 4x1 and 1x4 MUX/DMX was displayed in fig.24.

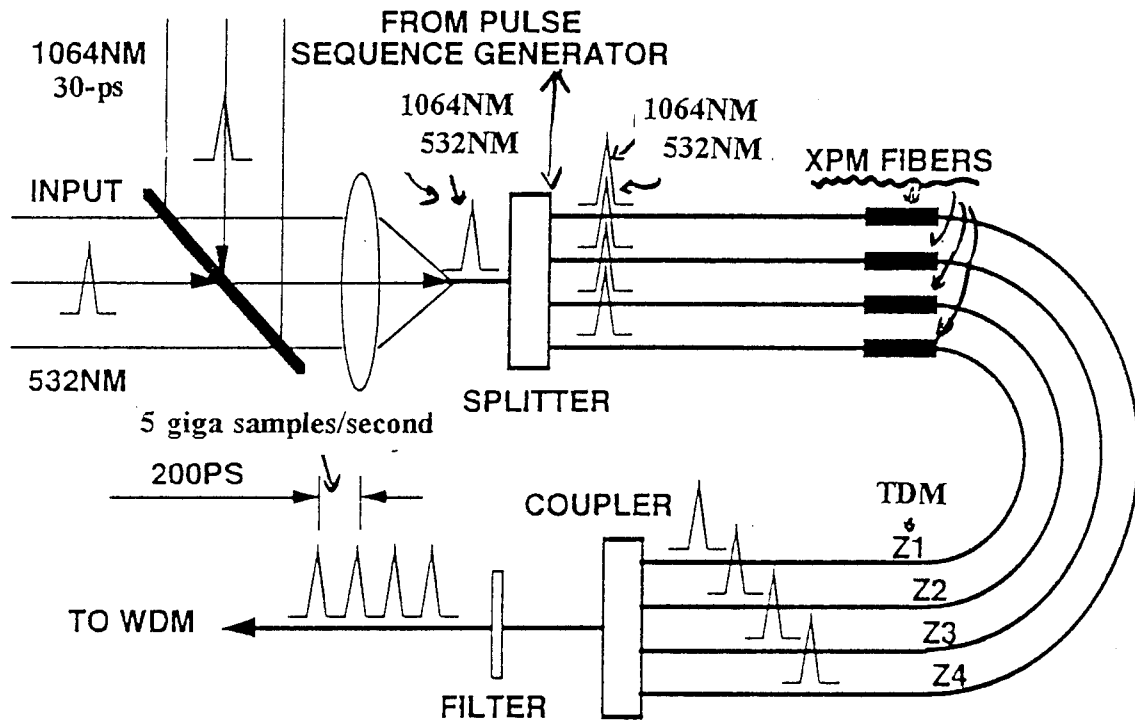


Fig.23 A schematic design of optical pulse sampling and clock using 1x4 and 4x1 fiber splitter (DMX) and coupler (MUX). The clocking pulse or time-divided multiplexing train was obtained using variable fiber lengths 1 cm difference in fiber length = 50-ps pulse separation. all beamsplitters (M) work at 45° incident angle. R is a rotator for laser pulses at 532 nm. Q is quarter wave plate; and PP is polarizing prism which combines clock pulse train and sampling pulse train into the same propagating direction with perpendicular polarization direction. Then, quarter wave plate converts two linearly perpendicularly polarized pulses trains into two opposite circularly polarized pulses trains.

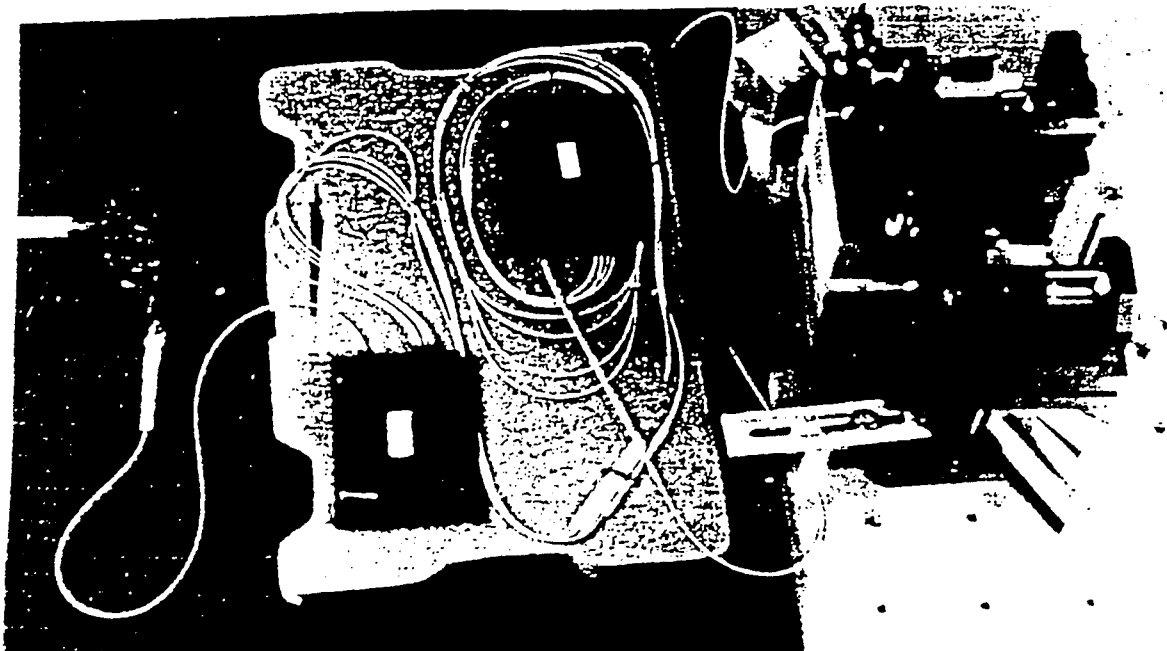


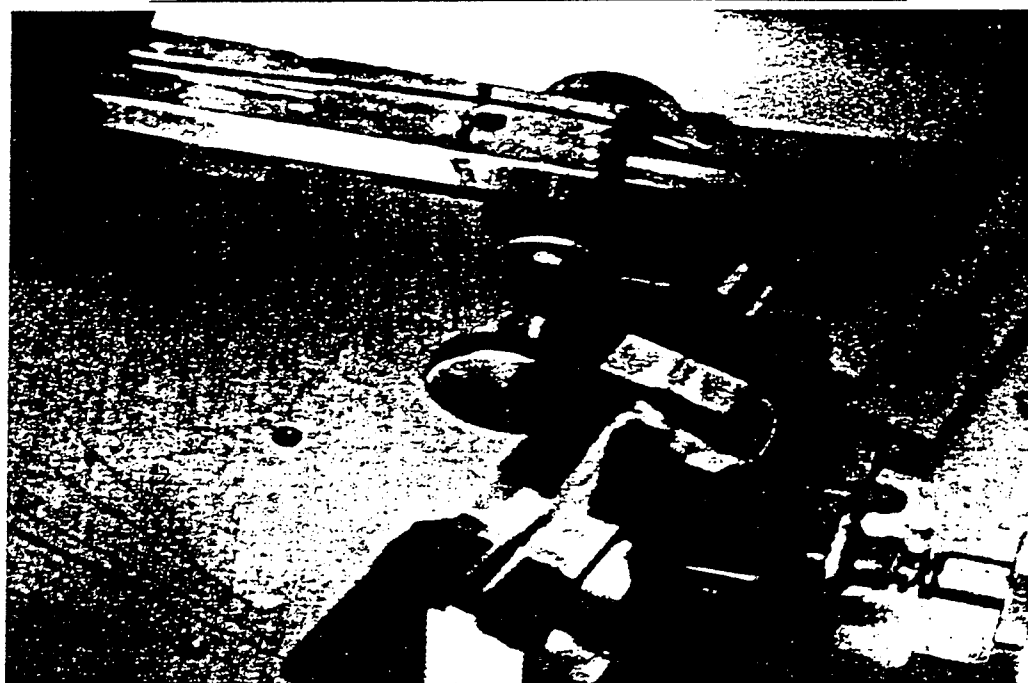
Fig.24 Photograph of optical pulse sampling and clock using 4x1 and 1x4 fiber MUX and DMX

The spectral distribution of the output pulse of the 532-nm carrier pulse after the XPM fiber and the spectrometer (WDM) can be expressed as:

$$w'_{532}(I_{1064}) = w_{532} + \delta w(\text{XPM}) = w_{532} + K I_{1064} = w_{532} + N \Omega(r)$$

where K is a proportional constant, N is an integer number from 0 -> 15, and  $\Omega(r)$  is the unit of spectral digitization which depends on the minimum resolution of the spectrometer. In this manner, the intensity of 1064-nm signal has been converted into a spectral/spatial distribution. After the WDM, a fiber bundle/waveguide MUX/DMX system has been used as discussed in figs.19 and 20.

A photograph of the experimental setup of an unary encoder with an equivalent 16 digital level using the fiber bundle is shown in fig.25.



UNINARY ENCODER, OUTPUT TO STREAK CAMERA

Fig.25 Photography of an unary encoder using fiber bundles based on design of figs.19 & 20

In fig.26a, a time-resolved streak camera measurement of the unary encoded TDM train is displayed and in fig.26b, a steady state image of the fiber bundle output from the unary encoder is displayed for the intensity calibration. From the cw measurement of fig.26b, the output intensity from these 16 fiber outputs was nearly the same for an uniform input beam. In fig.26a, the relative input intensity distribution from a 4-pulses train input of  $I_1:I_2:I_3:I_4$  was  $\sim 9:10:11:100$ . This pulse train intensity distribution was due to the control of the fiber/waveguide MUX/DMX as discussed in fig.20. Each pulse was separated by 200-ps apart in time. After the fiber bundle unary encoder, each pulse was digitized into a possible of 1 to 16 unary levels TDM with the pulse separation of 50-ps using 4-fibers per input pulse. The corresponding digitization levels for these 4 pulses were 10:11:12:16 as counted in fig.26a. In our digitization algorithm, for the relative input signal between 0 and 1 ( $1 \geq I_i > 0$ ), the unary encoded digitized output level will be assigned to be 1 ( $I_{out} = 1$ ); for  $2 \geq I_i > 1$ ,  $I_{out} = 2$ ; etc.; for any  $I_i > 15$ ,  $I_{out} = 16$ . A 5 Gigasamples/sec 4-bits (16 levels) XPM A/D has been demonstrated.

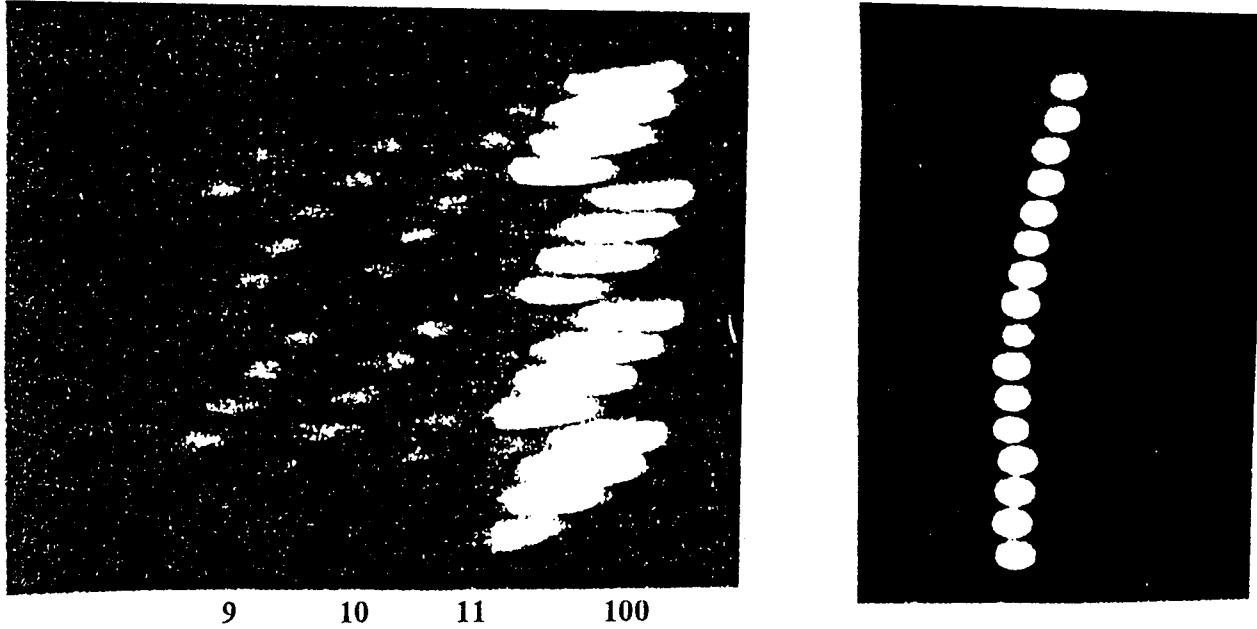


Fig.26 Demonstration of 5 Gigasamples/sec 4-bits XPM A/D  
(a) TDM measured by a 10-ps resolution streak camera to display unary encoded 4-pulse train. The relative input 4-pulses intensities were 9:10:11:100, the digitized outputs were 10:11:12:16.  
(b) Intensity uniformity calibration of the fiber bundle encoder using a steady state imaging.



## 8. Development of Compact fs/ps Semiconductor Diode Laser

In our previous and current experiments, a ps YAG and a fs Ti:sapphire laser were used. Both lasers are bulky, but available at our laboratory. They served to demonstrate our planned purpose for a laboratory demonstration of XPM A/D. For the future instrumentation application, a compact actively mode-locked picosecond semiconductor diode laser will be needed. The laser systems used for this program is shown in Table 1.

**Table 1      Laser System Used (or planned to be used) in XPM/A/D**

<u>Laser System</u>	<u>Pulse Duration</u>	<u>Energy</u>	<u>Repetition</u>	<u>Wavelength (nm)</u>
Nd:YAG	30 ps	100 mJ	10 Hz	1054, 532
Ti:sapphire	100 fs	10 nJ	80 MHz	800
Ps Diode Laser				
Oscillator	0.6-10 ps	100 pJ	1 GHz	830
Amplifier (being built)	10 ps	1 $\mu$ J	1 MHz	830

In a parallel effort, a ps diode laser has been assembled and tested as shown in fig.27. An AlGaAs semiconductor diode with anti-reflection surface coating and angled active layer to eliminate most internal reflection loss was used as the active medium. Two 0.85 NA microscope objectives, one 100% reflection back mirror at 850-nm, and one 30% transmission output coupler have been used to form the external laser cavity. A Spectra Diode Labs. model SDL-800 laser diode driver was used to provide the direct current for this diode laser. A HP function generator with frequency tuning from 0.1 MHz to 2 GHz was used to tune the modulation circuits separated by a T-Bias. Preliminary results of the laser output have been measured. The CW power-current characteristics without and with the external cavity are shown in fig.28.

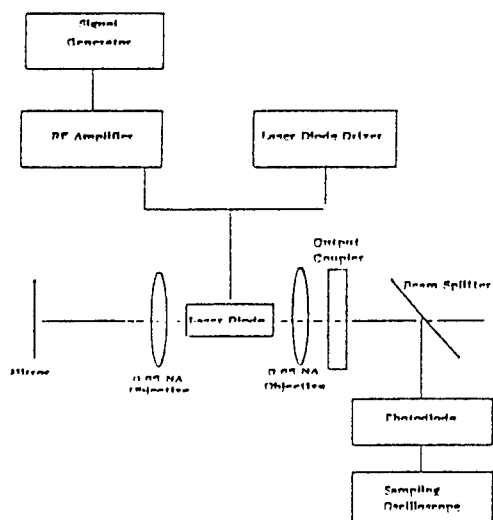


Fig.27 Schematic Diagram of Actively Mode-locked Semiconductor Diode Laser

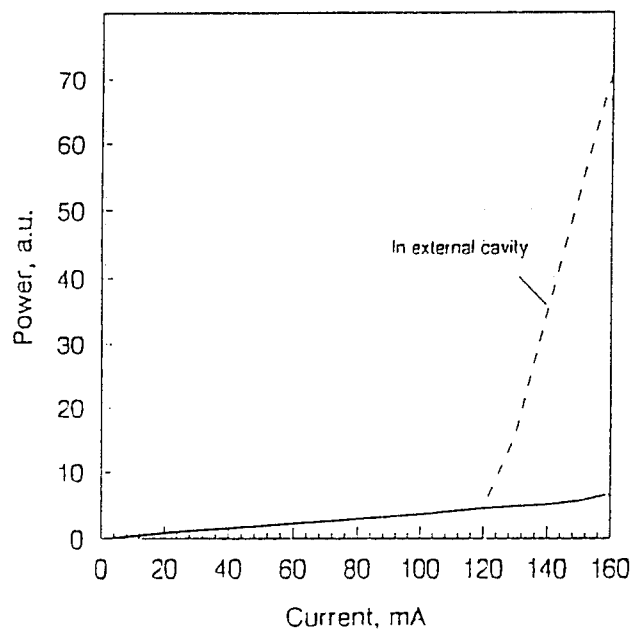


Fig.28 Power-current Characteristic of Laser  
Solid curve: No External Cavity  
Dashed curve: With External Cavity

Without the laser cavity, the laser diode operates as a traveling amplifier. The output power of the laser increases linearly as a function of the pump current. Due to the high optical loss in the active region, the stimulated emission did not take place without external cavity. With an external cavity, the gain overcomes the total loss at  $I > 120\text{-mA}$ , mode-locked picosecond laser pulse train has been obtained as shown in fig.29.

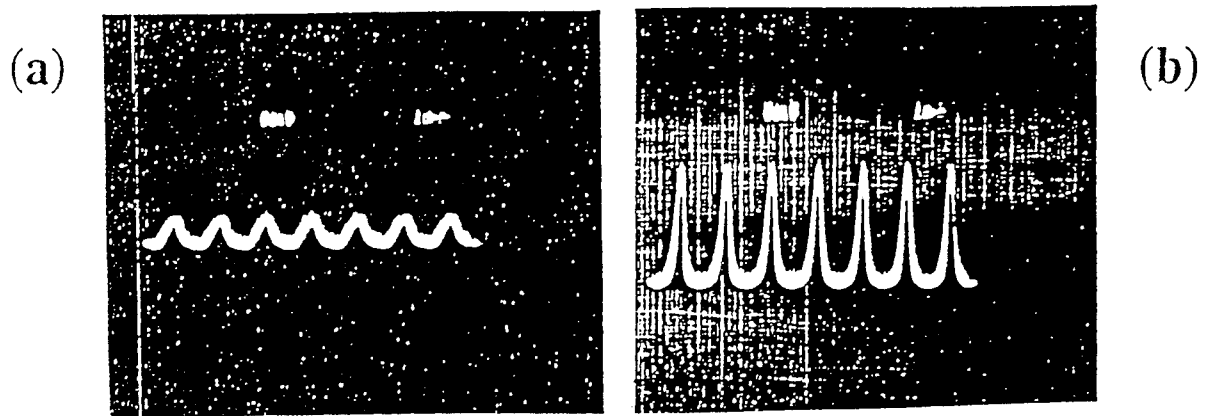


Fig.29 Photographs of Laser Output Train.  
Input Current = 130-mA; Modulation Frequency = 66 MHz; Modulation Amplitude = 1.25 V.  
(a) No External Cavity (Traveling wave amplifier)  
(b) With External Cavity (Picosecond operation)

Using the 2D interferometric amplitude correlator which is sensitive to the coherent component of the laser pulse, 0.6-ps pulse duration has been obtained. The compact ps semiconductor diode laser under development here has serves a starting point for the miniature of the future ultrafast optical A/D system. The pulse energy of 100-pJ is  $\sim 1,000$  times lower than the current XPM A/D required. An optical laser amplifier is needed to increase the pulse energy. This device is also being investigated. Two possible amplifier materials using either argon pump Ti:sapphire or diode laser pumped Cr:LiSAF regenerative amplifier is under study. The output performance of the laser and planned amplifier systems are shown in Table 2.

**Table 2 Specifications of Diode Laser Oscillators and Regenerative Amplifiers**

(a) Argon laser pumped Ti:sapphire amplifier      (b) Diode laser pumped Cr:LiSAF amplifier

(a)	Measured laser diode oscillator output	Expected argon ion laser pumped Ti:sapphire regenerative amplifier output
Wavelength	830 nm	830 nm
Energy/pulse	10-1 pJ	10-1 $\mu$ J
Average power	1 mW	400 mW
Pulse repetition rate	140 MHz - 1.5 GHz	1 MHz
Pulse width	0.6 ps	1-2 ps

(b)	Measured laser diode oscillator output	Expected diode laser pumped Cr:LiSAF regenerative amplifier output
Wavelength	830 nm	830 nm
Energy/pulse	10-1 pJ	10-1 $\mu$ J
Average power	1 mW	-
Pulse repetition rate	140 MHz - 1.5 GHz	10 kHz
Pulse width	0.6 ps	1-2 ps

## 9. Degenerative XPM (DXPM) and Polarization Instability

The main problem of this program was the development of a 4 bit XPM A/D converter. This was achieved for an input pulse energy requirement of  $\sim 100$ -nJ for a 4-bit (16 level) digitization. At a given pulse energy, the pulse intensity,  $I = \text{energy}/(\text{area} \times \text{duration})$ , requirement to the XPM spectral encoding can be expressed as

$$\delta\omega(\text{XPM}) \sim n_2 I z / \tau.$$

where  $n_2$  is the nonlinear index of refraction of the fiber,  $z$  is the fiber length between the signal and carrier pulses, and  $\tau$  is the pulse duration. To reduce the  $I$  requirement to lower levels with  $n_2$  and  $\tau$  remain to be constant, the interaction length  $z$  has to be increased. However, due to the material dispersion between two different wavelengths of the signal and carrier pulses used in XPM,  $z$  is limited to an effective interaction length (walk-off distance):  $z(\text{eff})$ . For instance, using 532-nm and 1064-nm as the XPM carrier and signal wavelengths in a silica glass fiber, the  $z(\text{eff})$  for a 20-ps pulse duration is  $\sim 26$  cm. Using  $n_2 \sim 10^{-13}$  esu and  $I \sim 10^9 \text{ W/cm}^2$  ( $10^7$  esu), the maximum XPM spectral shift is  $\sim 300$  GHz. where the  $z(\text{eff})$  can increase by a factor of 100, the  $I$  or the input energy required can be reduced by a factor of 100. The sensitivity of A/D can be greatly improved. DXPM<sup>38,39</sup> experiments have been carried out to test the concept where both the signal and carrier pulses have the same wavelength at orthogonal polarizations. From the dispersion consideration, the  $z(\text{eff})$  can be  $\rightarrow \infty$ . However, induced polarization stability occurred for the linearly polarized waves in short fibers and intrinsic fiber birefringence existed in long fibers. DXPM A/D process requires a further study to improve the sensitivity and accuracy.

### 9.1 Nonlinear Intensity Induced Polarization of Linearly & Circularly Polarized ps Laser Pulse

In optical fibers, the SPM and XPM processes are particularly important for the control of light in confined and guided core of fibers<sup>[22-26]</sup>. The nonlinear processes in optical fibers affect

not only the spectral and temporal structures of the propagating optical pulses, but also their polarization states. The intensity-induced polarization changes of an optical wave propagating in single-mode optical fibers were observed experimentally without a satisfactory theoretical model<sup>[27-39]</sup>. The relation between vector rotation and depolarization in non-birefringent optical fibers is under investigation. The effects of intensity on the state of polarization have been observed for circularly and linearly polarized optical pulses propagating in a single mode optical fiber. The state of circular polarization is found to be more stable than the state of linear polarization for short non-birefringent single mode optical fibers. We have a model based on SPM and XPM to explain the measured preservation of the circular polarization and the depolarization of linearly polarized laser pulses in the optical fibers.

The polarization of laser pulses of 30-ps duration at 532 nm propagating in single-mode optical fibers have been measured using circularly and linearly polarized as shown in fig.30. The pulses were obtained from a frequency doubled mode locked Nd:YAG laser at a repetition rate of 10 Hz. After the polarizer P1, the input laser pulses were linearly polarized to a ratio better than 400:1. Using a quarter wave plate, these pulses were converted into circularly polarized ones. By changing the direction of the optical axes of the quarter wave plate, one can convert the laser pulses to be either right-handed or left-handed circularly polarized. The circularly polarized laser pulses were then coupled into and out of optical fiber. A beam displacing prism was used after the second quarter wave plate to separate these two orthogonal linear polarizations. Depending on the polarization state, one output pulse was divided into two pulses (defined as I and II), which have orthogonal polarization directions. Pulses I and II represent the part of polarization state unchanged and the part transferred to the orthogonal polarized mode, respectively. The energies of pulses I and II were measured using a cooled CCD camera system. Neutral density filters were placed in front of the CCD camera to adjust the intensity of laser

pulses I and II, respectively.

The data plots (a) and (b) in Fig. 31 show how the degree of polarization for circularly and linearly polarized laser pulses propagating in a fiber change with different input laser pulse energy. The degree of polarization for a circularly polarized input laser pulse was preserved to be  $> 0.9$  when the laser pulse energy was varied from 40 pJ to 60 nJ. The energy range covering three orders of magnitude until the input tip of the optical fiber was burned. Similar results were observed when the length of the optical fiber was increased from 0.5 m to 4 m. The states of polarization for circularly polarized input laser pulses were preserved in a non-birefringent single mode optical fiber.

When linearly polarized laser pulses were coupled into a one meter non-birefringent single mode optical fiber, the degree of linear polarization quickly depolarized when the energy of the input laser pulse was  $> 6$  nJ. SPM and XPM processes are responsible for the stability of the circularly polarized optical pulses and the depolarization of the linearly polarized pulses at high intensities. The theoretical calculation was displayed as solid lines in Fig.31.

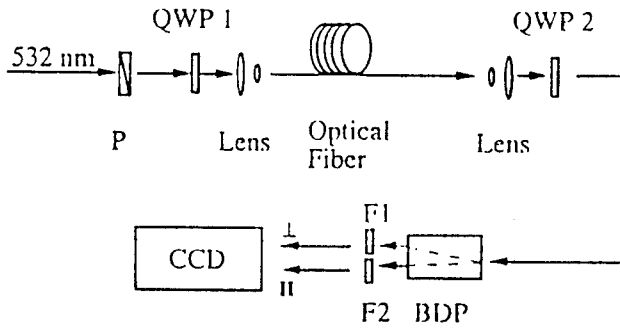


Fig.30 Experimental setup for measuring the stability of the circular and linear polarization states. BDP; beam displacing prism(polarizing prism), F's neutral-density filters.

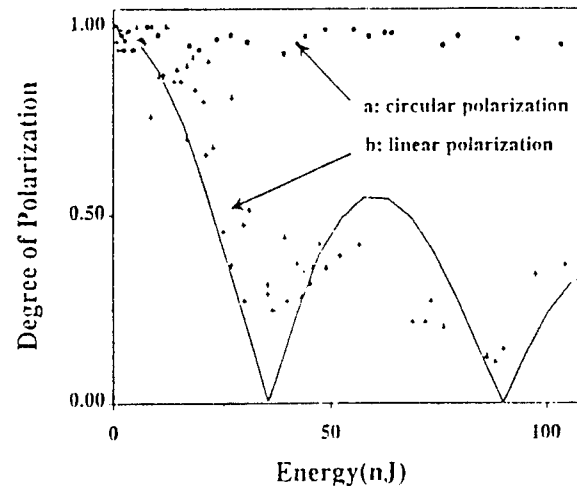


Fig.31 The measured results of the polarization stabilities for different polarization states depending on the laser pulse intensities(pulse Energies). The curve is the theoretical fitting.

## 9.2 Single-pulse DXPM from a Picosecond Circularly Polarized Laser Pulse

XPM process was demonstrated using two optical pulses with different wavelength and different polarizations. Two physically separated optical pulses were always coupled into a nonlinear medium to let the intense one(as pump) modulate the weak one(as probe). The temporal and spectral feature of the probe can be changed with the presence of the pump beam. In principal, the two polarization components in a single pulse can act as two laser pulses with the some phase and amplitude difference. XPM between two polarization components of a single laser pulse should be observable if the two polarization states are stable in an optical fiber.

The experimental arrangement of the single-pulse DXPM is shown in Fig.32a. One-meter non-birefringent single mode optical fiber and 30 ps laser pulses at 532 nm were used. After the polarizer P, the input laser pulse was linearly polarized to a ratio better than 400 to 1. The elliptically polarized laser pulse was obtained by adjusting the relative angle of optical axes between the quarter wave plate QWP1 and the polarizer P. When this angle is  $45^\circ$ , a circularly polarized laser pulse is produced. The intensities of the two circular polarization components of the single elliptical laser pulse was set with a ratio of 100 to 1.

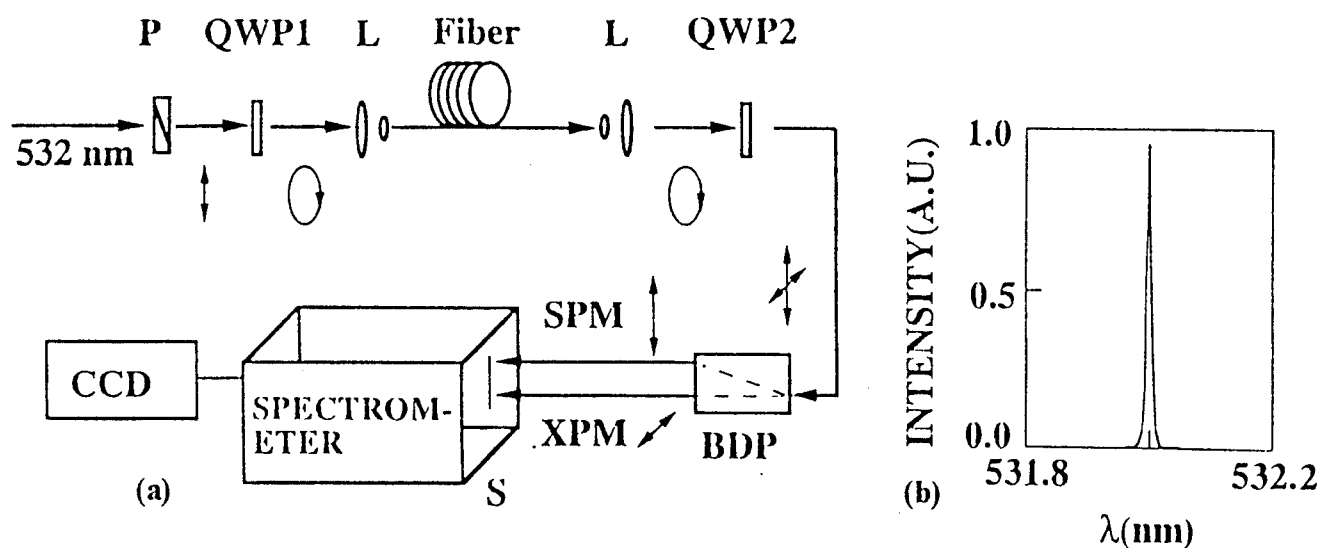


Fig.32 Single-pulse DXPM in Optical Fibers

(a) Schematic of experimental setup. L: lens, QWP: quarter wave plate

(b) Measured spectrum of the input laser pulse: FWHM bandwidth  $\sim 0.2\text{\AA}$

The intense component acted as a pump pulse while the other one as a probe pulse. Two circular polarization components co-propagated through optical fiber and each one remained in its own polarization state without exchange of energy. After the second quarter wave plate QWP2, these two components were converted into two perpendicular linear polarization ones. After that, a polarizing prism BDP was used to separate the two linear polarization components and the spectra were measured. The input laser spectrum had a FWHM bandwidth  $\sim 0.2\text{A}$ . The output spectra of two polarization components of a single 532 nm laser pulse were measured for different coupled pulse energies. Fig.33 displays the normalized spectra at an input pulse energy of 30-nJ. Fig.33a is the output spectra of the pump component, while Fig.33b is the spectra of the probe. The spectral of the pump is attributed to the typical SPM process. The spectral broadening of the probe component is attributed to the XPM process caused by pump and the interference between them. Using the nonlinear coupling equations for circularly polarized pulses, the theoretical fitting of the SPM and XPM spectra are shown in Fig.34. After introducing the interference between SPM and XPM, good agreements have been obtained between with the measured XPM spectrum in Fig.33b to the calculated spectrum in fig.34c.

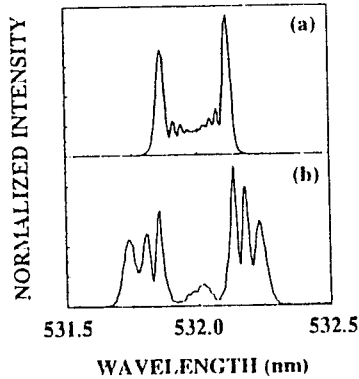


Fig.33 Measured spectra of single 30-nJ elliptically polarized laser pulse with a duration of 30 ps propagating in a 1-m nonbirefringent single-mode optical fiber. The intensity ratio of the pump component to the probe was 100 to 1. (a), (b) Spectra of pump and probe components, respectively.

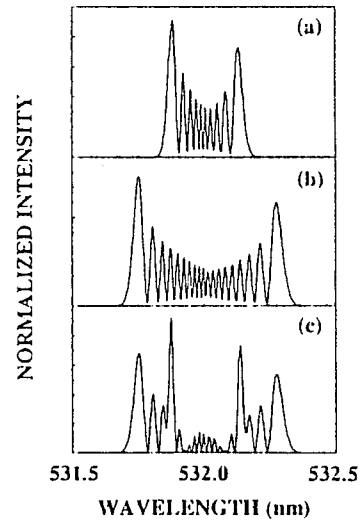


Fig.34 Theoretical calculation of SPM and DXPM spectra for a single elliptically polarized laser pulse at the same pulse energy of 30 nJ,  $n_2 = 1.3 \times 10^{-16} \text{ cm}^2/\text{W}$ , fiber length 1 m, and fiber core diameter 2.5  $\mu\text{m}$ . The intensity ratio of pump to probe is 100 to 1. (a), (b) Spectra of pump and probe components, respectively. (c) Spectrum considering interference between the probe and a small portion (0.5%) of the pump.



## 10. Summary: Problems and Future Direction

We have successfully demonstrated a 5 Giga-samples/sec 16-level XPM A/D system. There are still many issues to be solved for the final implementation of this unary encoded XPM A/D algorithm. Based on the study of the induced stability discussed in section 9, a polarization controlled all optical amplifier to improve A/D sensitivity by reducing the minimum pulse energy requirement from 10-nJ to 1-pJ. A patent disclosure has been filed. Furthermore, using our previously patented algorithm of the induced optical deflector<sup>40</sup>, ultrafast low-level input signals for both cw and pulsed operation in  $\sim$  mW power can be digitized<sup>11</sup> as shown in fig.35.

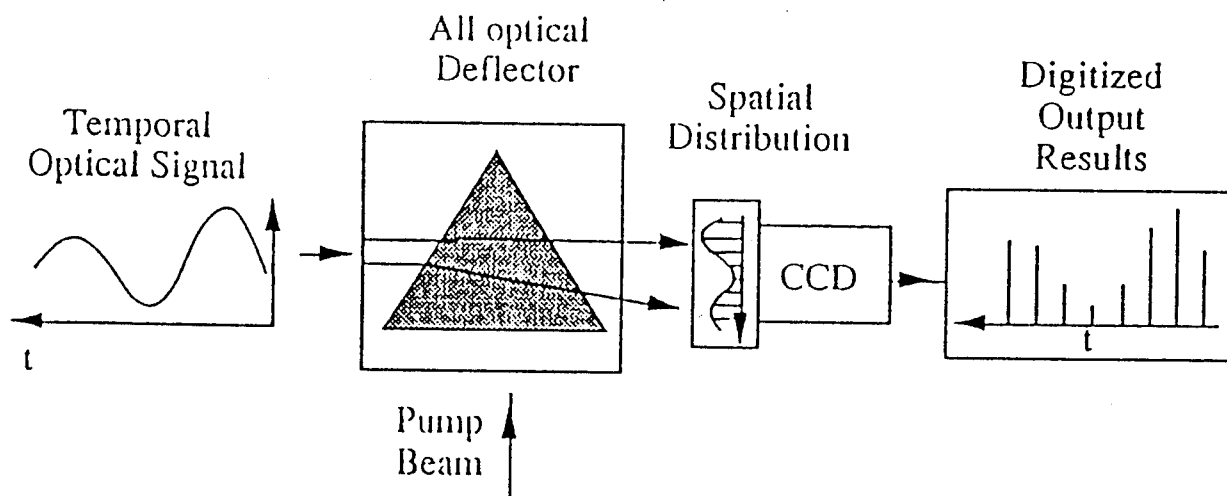


Fig.35 A schematic of an ultrafast waveform digitization for low-level input signal using induced-beam deflection principle

There are five immediate issues for the 4-bit ultrafast optical XPM A/D which requires the further study.

They are :

a) Accuracy of XPM Spectral Encoding A/D Using Circularly Polarized Laser Pulse:

Experimental measurements of the polarization ratio of linearly and circularly polarized laser pulses propagating in optical fibers indicated that circularly polarized laser pulses will be helpful to study polarization sensitive processes because the polarization state can be preserved at high intensity. The dependence of XPM spectra as a function of an input laser pulse intensity should be studied. The effect of XPM spectral distribution on polarization stability for the encoded A/D algorithm should be investigated. In a standard XPM analysis, the broadened XPM spectrum of the carrier pulse  $\delta\omega_2(\text{XPM}) \sim |E_1|^2$ . In theory, when the polarization state of the signal pulse  $E_1$  is changing with respect to the carrier pulse  $E_2$ , the effective  $\delta\omega_2(\text{XPM})$  can be varied from a factor between 2/3 to 2 depending on the polarization states of  $E_1$  and  $E_2$  are either in perpendicular or in parallel, respectively. Using the results shown in fig.31, the polarization state of a linearly polarized signal was found to vary as the incident laser intensity. This polarization instability can greatly reduce the accuracy of A/D using DXPM. Since the circular polarization states are stable, to the induced polarization change, the accuracy of A/D can be improved by a factor of 3.

b) Accuracy Improvement of XPM A/D with Better Pulse Energy Control

One of the accuracy limitation of 4-bits resolution with our current XPM spectral measurements is the fluctuation of input pulse energy control of mode-locked YAG laser system. The XPM spectral shift of > 200 channel has been obtained as shown in fig.10. With the state-of-the-art mode-locked lasers, e.g. ps Ti:sapphire laser, the pulse energy fluctuation can be improved by a factor of ten. In together with the pulse polarization control in a), 64-levels (6 bits) could be

obtain with the current encoding algorithm.

c) New Encoding Algorithms

In our current XPM A/D spectral encoding algorithm, a 4-bit resolution has been achieved. A further study of the XPM spectral encoding algorithms, e.g. modulated spectral distribution, may improve the bit accuracy.

d) Spectral Modification of XPM Oscillatory Spectrum to Singular Output

In our current demonstration unit, an unary encoding algorithm was used due to the oscillation nature of the XPM spectrum. In addition, a spatial mask has been designed to convert the priority encoded optical signals into binary encoded optical signals. Both cases are bulky. An algorithm on ultrafast optical comparator is needed to improve the sensitivity from the unary - > binary coding. A time-gated XPM spectrum is being developed which may modify XPM oscillating spectra into a distinct spectral shift as our original plan in fig.4. In this many, encoding algorithm can be converted from unary coding to priority coding. A detail analysis of this time gated modification will be submitted in a renewal proposal.

e) Compact/Stable ps Laser Sources

In our demonstration unit, an intense optical signal is needed as the pump beam to be digitized in the XPM process. The dimension of the laser used is not realistic for the practical applications. A laser amplifier to increase peak power of a compact ps diode laser source will be proposed to be studied in the future.

A renewal proposal will be submitted to address the above five issues of XPM A/D with better sensitivity, more accuracy, lower cost, and compact package.

## 11. References

- [1]. M.J. LaGasse, D. Liu-wong, J.G. Fujimoto and H.A. Haus, Opt. Lett. **14**, 311-313, (1989)
- [2]. Y. Kimura, K. I. Kitayama, N. Shibata and S. Seikai, Electron. Lett. **22**, 277 (1986).
- [3]. J. -M. Jeong and M. E. Marhic, Opt. Comm. **85**, 430 (1991).
- [4]. A. S. Davison and I. H. White, Opt. Lett. **14**, 802 (1988).
- [5]. M. E. Marhic, C. H. Hsia and J. -M. Jeong, Electron. Lett. **27**, 27 (1991).
- [6]. T. Morioka, M. Saruwatari and A. Takada, Electron. Lett. **27**, 210 (1991).
- [7]. J. -M. Jeong and M. E. Marhic, Opt. Comm. **91**, 115-122 (1992).
- [8]. A. M. Weiner, J. P. Heritage and J. A. Salehi, Opt. Lett. **13**, 300-302 (1988).
- [9]. M. A. Flavin and J. L. Horner, Appl. Opt. **28**, 1692-1696 (1989).
- [10]. B. L. Shoop and J. W. Goodman, Appl. Opt. **31**, 5654-5660 (1992).
- [11]. P. P. Ho, Q. Z. Wang, Q. D. Liu , Disa Liu, and R. R. Alfano, Optoelectronic Signal Processing for Phased-array Antennas IV, SPIE Proc. Vol. **2155**, 157-160 (1994).
- [12]. P. P. Ho, Q. Z. Wang, Q. D. Liu , Disa Liu, and R. R. Alfano, Optoelectronic Signal Processing for Phased-array Antennas IV, SPIE Proc. Vol. **2155**, 37-40 (1994).
- [13]. R. R. Alfano ed., The Supercontinuum Laser Source (Springer-Verlag, New York), 1989.
- [14]. R. R. Alfano and Shapiro, Phys. Rev. Lett. **24**, 584, 592, 1217 (1970).
- [15]. R. Fork, C. Shank, C. Herliman, R. Yen and W. J. Tomlinson, Opt. Lett. **8**, 1 (1983).
- [16]. G. Yang and Y. R. Shen, Opt. Lett. **9**, 510 (1984).
- [17]. R. H. Stolen and Chinlon Lin, Phys. Rev. A **17**, 1448 (1978).
- [18]. E. P. Ippen, C. V. Shank and T. K. Gustafson, Appl. Phys. Lett. **33**, 1765 (1974).
- [19]. Q. Z. Wang, Q. D. Liu, P. P. Ho and R. R. Alfano, Opt. Lett. **19**, 1636 (1994).
- [20]. R. R. Alfano, Q.X. Li, T. Jimbo, J. T. Manassah, and P. P. Ho, Opt. Lett. **11**, 626 (1986)
- [21]. C. C. Yang and Alex J. S. Wang, J. Opt. Soc. Am. B **9**, 682 (1992).

- [22] M. N. Islam, L. F. Mollenauer, R. H. Stolen, J. R. Simpson, H. T. Shang, *Opt. Lett.* **12**, 625 (1987).
- [23] P. L. Baldeck, R. R. Alfano and G. P. Agrawal, *Appl. Phys. Lett.* **52**, 1939 (1988).
- [24] Q. Z. Wang, Q. D. Liu, P. P. Ho and R. R. Alfano, *J. Opt. Soc. Am. B* **11**, 1084(1994)
- [25] Q. Z. Wang, P. P. Ho and R. R. Alfano, *Opt. Lett.* **15**, 1023 (1990).
- [26] K. J. Blow, N. J. Doran and B. P. Nelson, *Opt. Lett.* **10**, 393 (1985)
- [27] B. Crosignani, B. Daino, P. D. Porto, *J. Opt. Am. B*, **3**, 1120-1123 (1986).
- [28] B. Crosignani, P. D Porto, *Opt. Acta*, **32**, 1251-1258 (1985).
- [29] H. G. Winful, *Appl. Phys. Lett.* **47**, 213-215 (1985).
- [30] H. G. Winful, *Opt. Lett.* **11**, 33-35 (1986).
- [31] C. Y. Menyuk, and P. K. A. Wai, *J. Opt. Am. B*, **11**, 1035-1039 (1994).
- [32] P. D. Maker, R. W. Terhune, and C. M. Savage, *Phys. Rev. Lett.* **12**, 507-509 (1964).
- [33] A. Owyong, R. W. Hellwarth, and N. George, *Phys. Rev. B*, **5**, 628-633 (1972).
- [34] R. Kashyap, and N. Finlayson, *Opt. Lett.* **17**, 405-407 (1992).
- [35] S. Trillo, S. Wabnitz, R. H. Stolen, G. Assanto, C. T. Seaton, and G. I. Stegeman,  
*Appl. Phys. Lett.* **49**, 1224-1226 (1986).
- [36] S. F. Feldman, D. A. Weinberger, and H. G. Winful, *Opt. Lett.* **15**, 311 (1990).
- [37] E. Lichtman, R. G. Waarts, A. A. Friesem, and S. Tang, *Appl. Opt.* **28**, 4056-4058).
- [38] Q. D. Liu, J. T. Chen, Q. Z. Wang, P. P. Ho and R. R. Alfano, *Optics Letters*,  
vol. **20**, pp542-544 (1995).
- [39] Q.Liu, J.Chen, P.Ho, R.Alfano, *IEEE Photonics Tech.Letters*, vol.7, pp517-519, (1995).
- [40] R. R. Alfano, Y. Li, P. Baldeck, "Transient optical circuits", US patent # 5,126,874,  
June 30 (1992).

## 12. Research Staff in this Program

Prof. P. Ho                      Professor of EE

In charge of the overall program, 10% effort

Prof. R. Alfano                Distinguished Professor of Science & Engineering

In charge of ultrafast optics and laser research, 5% effort

Dr. Q. Z. Wang               Research Associate

In charge of laboratory operation and computer analysis, 100% effort, 8/92-3/94

Dr. J. T. Chen                Research Associate

In charge of laboratory operation, 100% effort, 4/94-7/95

Dr. K. Setkus                 Research Associate

Mode-locked semiconductor diode laser development, 25% effort

Mr. Q. D. Liu                 Ph.D. Graduate Research Assistant

Laboratory operation and data analysis, 100% effort

Ms. Disa Liu                 Ph.D. Graduate Research Assistant (supported by NSF)

System simulation and encoding algorithms, 1/93-6/94

### 13. Accomplishments and Publication List Acknowledging RADA/ARAP Support

#### TECHNICAL ACCOMPLISHMENTS

- \* Demonstrated a 1x4 waveguide/fiber DMX using a streak camera to simulate a carrier/signal train separated by 200-ps (5 Gigasample) test. Used 1x4 and 4x1 splitter/coupler with variable fiber lengths to achieve a 50-ps/division (20 Gb/s).
  
- \* Repeated XPM experiments and improved XPM spectral shifted channels from 5 -> 200. Observed modulated XPM spectrum and redesigned the encoding algorithm from binary to unary. Determined the linearity of a 4-bit (16 digital levels) XPM A/D intensity spectral encoding.
  
- \* Measured and modeled SPM and XPM spectral distribution of ps/fs propagating through optical fibers. Determined XPM Fiber mode coupling requirements.
  
- \* Designed, built, and tested a ML semiconductor diode laser with duration  $\sim 0.6$ -ps at  $\sim 1$  GHz. Received parts to assemble and test an amplifier with output energy  $\sim 1$ - $\mu$ J at  $\sim 100$ -KHz.
  
- \* Measured femtosecond XPM in isotropic and polarization preserved fibers and determined  $\Delta\omega$   $\sim$  Intensity from single pulse DXPM and effective fiber length.
  
- \* Measured/modeled vector properties of ultrashort laser pulse propagating in fibers. Determined circularly polarized mode is stable of pulse propagation in fibers.

Publication List Acknowledging RADA/ARAP Support

- [1]. Q. D. Liu, J. T. Chen, Q. Z. Wang, P. P. Ho and R. R. Alfano, " Single-pulse degenerate-cross-phase modulation in non-birefringent single-mode optical fibers", Optics Letters, vol. **20**, pp542-544 (1995).
- [2]. Q. D. Liu, J. T. Chen, P. P. Ho and R. R. Alfano, " Polarization stability of circularly polarized laser pulses propagating in nonbirefringent single mode optical fibers". IEEE Photonics Technology Letters, vol. **7**, pp517-519, (1995).
- [3]. Q. Z. Wang, Q. D. Liu, P. P. Ho, E. K. Walge and R. R. Alfano, "High resolution spectra of cross-phase modulation in optical fibers," Optics Letters **19**, pp 1636-1638 (1994).
- [4]. Q. Z. Wang, Q. D. Liu, Disa Liu, P. P. Ho and R. R. Alfano, "High resolution spectra of self-phase modulation in optical fibers," J. Opt. Soc. Am. B **11**, 1084-1089 (1994).
- [5]. J. T. Chen, Q. D. Liu, P. P. Ho and R. R. Alfano, " Depolarization of picosecond ~~linear~~ pulses by asymmetric nonlinearity in optical fibers", Journal of Optical Society of America, B12, pp907-912 (1995)
- [6]. P. P. Ho, Q. Z. Wang, Q. D. Liu, and R. R. Alfano, "High resolution spectra of cross-phase modulation for an A/D converter," SPIE **2155**, pp37-40 (1994).
- [7]. P. P. Ho, Q. Z. Wang, Q. D. Liu, and R. R. Alfano, "Induced beam deflection for ultrafast low-signal-level optical waveform digitization," SPIE **2155**, pp157-161 (1994).



## **PRESENTATIONS AND PROGRAM REVIEWS:**

- [1]. Q. D. Liu, L. Shi, P. P. Ho and R. R. Alfano, " Vector property of femtosecond laser pulse propagating in non-birefringent single-mode optical fibers," CLEO/QELS, Baltimore, MD, May (1995)
- [2]. Attended and presented a talk (Prof. P. Ho) at the 1995 ARPA Optics Review at Big Sky, Montana, 7/31-8/3 (1995).
- [3]. Q. Z. Wang, Q. D. Liu, P. P. Ho, E. Walge and R. R. Alfano, "Waveguide multiplexer and de-multiplexer signal encoding for ultrafast XPM A/D converter" has been presented at the 1994 OSA Annual Meeting in Dallas in 10/1994.
- [4]. P. P. Ho, Q. Z. Wang, Q. D. Liu , Disa Liu, and R. R. Alfano, "High resolution spectra of cross-phase modulation for A/D converter," Optoelectronic Signal Processing for Phased-array Antennas IV, SPIE Meeting at Los Angeles, Jan. (1994).
- [5]. P. P. Ho, Q. Z. Wang, Q. D. Liu , Disa Liu, and R. R. Alfano, "Induced Beam Deflection for Ultrafast Low-signal Level Optical Waveform Digitization," Optoelectronic Signal Processing for Phased-array Antennas IV, SPIE Meeting at Los Angeles, Jan. (1994).
- [6]. Attended and presented a talk (Dr. Q. Wang) at the 1994 ARPA Optics Review at Monterey, CA, in June, 1994.
- [7]. Presented a paper entitled "Ultrafast XPM A/D converter" at the 4th Annual 1994 IEEE Mohawk Valley Section "Dual-use technology & applications", May 1994.
- [8]. Attended and presented a talk (Prof. P. Ho) at the 1993 ARPA Optics Review at Hilton Island, SC, Feb. 1993.

# DISTRIBUTION LIST

addresses	number of copies
ROME LABORATORY/OCPC ATTN: JAMES L. DAVIS 25 ELECTRONIC PKY ROME NY 13441-4515	5
THE CITY COLLEGE OF THE CITY UNIV OF NY CENTER FOR ADV TECHNOLOGY CONVENT AVE & 138TH STREET NEW YORK NY 10031	5
ROME LABORATORY/SUL TECHNICAL LIBRARY 26 ELECTRONIC PKY ROME NY 13441-4514	1
ATTENTION: DTIC-DCC DEFENSE TECHNICAL INFO CENTER 8725 JOHN J. KINGMAN ROAD, STE 0944 FT. BELVOIR, VA 22060-6218	2
ADVANCED RESEARCH PROJECTS AGENCY 3701 NORTH FAIRFAX DRIVE ARLINGTON VA 22203-1714	1
NAVAL WARFARE ASSESSMENT CENTER GIDEP (QA50) ATTN: RAYMOND TADPO5 PO BOX 8000 CORONA CA 91718-8000	1
WRIGHT LABORATORY/AAAI-2, BLDG 635 2135 AVIONICS CIRCLE WRIGHT-PATTERSON AFB OH 45433-7301	1
AFIT ACADEMIC LIBRARY/LOEE 2950 P STREET AREA B, BLDG 642 WRIGHT-PATTERSON AFB OH 45433-7765	1

WRIGHT LABORATORY/MLPO 1  
ATTN: R. L. DENISON  
BLDG 651  
3005 P STREET, STE 6  
WRIGHT-PATTERSON AFB OH 45433-7707

WRIGHT LABORATORY/MTE, BLDG 653 1  
2977 P STREET, STE 6  
WRIGHT-PATTERSON AFB OH 45433-7739

AUL/LSE 1  
BLDG 1405  
600 CHENNAULT CIRCLE  
MAXWELL AFB AL 361126424

US ARMY SPACE & STRATEGIC 1  
DEFENSE COMMAND  
CSSD-IM-PA  
PO BOX 1500  
HUNTSVILLE AL 35807-3801

NAVAL AIR WARFARE CENTER 1  
6000 E. 21ST STREET  
INDIANAPOLIS IN 46219-2189

COMMANDER, TECHNICAL LIBRARY 1  
4747000/C0223  
NAVAIRWARCENWPNDIV  
1 ADMINISTRATION CIRCLE  
CHINA LAKE CA 93555-6001

US ARMY MISSILE COMMAND 2  
AMSMI-RO-CS-R/DOCUMENTS  
RSIC BLDG 4484  
REDSTONE ARSENAL AL 35898-5241

ADVISORY GROUP ON ELECTRON DEVICES 1  
1745 JEFFERSON DAVIS HWY  
SUITE 500  
ARLINGTON VA 22202

LOS ALAMOS NATIONAL LABORATORY 1  
PO BOX 1663  
REPORT LIBRARY, P364  
LOS ALAMOS NM 87545

AEDC LIBRARY 1  
TECHNICAL REPORTS FILE  
100 KINDEL DRIVE, SUITE C211  
ARNOLD AFB TN 37389-3211

AFIWC/MSO 1  
102 HALL BLVD, STE 315  
SAN ANTONIO TX 78243-7016

DIRNSA 1  
R509  
9800 SAVAGE ROAD  
FT MEADE MD 20755-6000

NSA/CSS 1  
K1  
FT MEADE MD 20755-6000

PHILLIPS LABORATORY 1  
PL/TL (LIBRARY)  
5 WRIGHT STREET  
HANSCOM AFB MA 01731-3004

THE MITRE CORPORATION 1  
ATTN: E. LAURE  
0460  
202 BURLINGTON RD  
BEDFORD MA 01732

OUSDC(P)/DTSA/DUTO 2  
ATTN: PATRICK G. SULLIVAN, JR.  
400 ARMY NAVY DRIVE  
SUITE 300  
ARLINGTON VA 22202

ROME LABORATORY/ERAA 1  
ATTN: DAVID D. CURTIS  
HANSCOM AFB, MA 01731-5000

ROME LABORATORY/ERO 1  
ATTN: RICHARD PAYNE  
HANSCOM AFB, MA 01731-5000

ROME LABORATORY/EROC  
ATTN: JOSEPH P. LORENZO, JR.  
HANSCOM AFB, MA 01731-5000

1

ROME LABORATORY/EROP  
ATTN: JOSEPH L. HORNER  
HANSCOM AFB, MA 01731-5000

1

ROME LABORATORY/EROC  
ATTN: RICHARD A. SOREF  
HANSCOM AFB, MA 01731-5000

1

ROME LABORATORY/ERXE  
ATTN: JOHN J. LARKIN  
HANSCOM AFB, MA 01731-5000

1

ROME LABORATORY/ERDR  
ATTN: DANIEL J. BURNS  
525 BROOKS RD  
ROME NY 13441-4505

1

ROME LABORATORY/IRAP  
ATTN: ALBERT A. JAMBERDINO  
32 HANGAR RD  
ROME NY 13441-4114

1

ROME LABORATORY/DCP  
ATTN: BRIAN M. HENDRICKSON  
25 ELECTRONIC PKY  
ROME NY 13441-4515

1

ROME LABORATORY/OCPC  
ATTN: GREGORY J. ZAGAR  
25 ELECTRONIC PKY  
ROME NY 13441-4515

1

ROME LABORATORY/C3BC  
ATTN: ROBERT L. KAMINSKI  
525 BROOKS RD  
ROME NY 13441-4505

1

ROME LABORATORY/OCP 1  
ATTN: JAMES W. CUSACK  
25 ELECTRONIC PKY  
ROME NY 13441-4515

ROME LABORATORY/OCP 1  
ATTN: JOANNE L. ROSSI  
25 ELECTRONIC PKY  
ROME NY 13441-4515

ROME LABORATORY/OCPA 1  
ATTN: ANDREW R. PIRICH  
25 ELECTRONIC PKY  
ROME NY 13441-4515

ROME LABORTORY/OCP 1  
ATTN: RICHARD J. MICHALAK  
25 ELECTRONIC PKY  
ROME NY 13441-4515

NY PHOTONIC DEVELOPMENT CORP 1  
MVCC ROME CAMPUS  
UPPER FLOYD AVE  
ROME, NY 13440

***MISSION***  
***OF***  
***ROME LABORATORY***

Mission. The mission of Rome Laboratory is to advance the science and technologies of command, control, communications and intelligence and to transition them into systems to meet customer needs. To achieve this, Rome Lab:

- a. Conducts vigorous research, development and test programs in all applicable technologies;
- b. Transitions technology to current and future systems to improve operational capability, readiness, and supportability;
- c. Provides a full range of technical support to Air Force Materiel Command product centers and other Air Force organizations;
- d. Promotes transfer of technology to the private sector;
- e. Maintains leading edge technological expertise in the areas of surveillance, communications, command and control, intelligence, reliability science, electro-magnetic technology, photonics, signal processing, and computational science.

The thrust areas of technical competence include: Surveillance, Communications, Command and Control, Intelligence, Signal Processing, Computer Science and Technology, Electromagnetic Technology, Photonics and Reliability Sciences.